# Calculating the static and dynamic hyperpolarizabilities of methyl oxirane with the Numerical Liouville Approach

by

Reese Sanders

B.S., Rochester Institute of Technology, 2024

---

A THESIS

submitted in partial fulfillment of the
requirements for the degree

MASTER OF SCIENCE

Department of Physics
College of Arts and Sciences

KANSAS STATE UNIVERSITY
Manhattan, Kansas

2026

Approved by:

Major Professor
Loren Greenman

# Copyright

# Abstract

Since its conception, nonlinear optics has proved to be a crucial tool for physicists across the discipline. Ultrafast researchers employ nonlinear optics to produce high harmonic pulses, and biophysicists apply nonlinear imaging techniques to image organic systems without the need for tagging the system. In this thesis, we investigate the fundamental nonlinear properties known as the hyperpolarizabilities for hydrogen fluoride and methyl oxirane. To calculate these, we numerically solve the Liouville equation for the case of the molecule in an oscillating field. From these solutions we extract the induced dipole, whose Fourier transform we fit to the appropriate nonlinear contributions to derive the hyperpolarizabilities.

Using hydrogen fluoride, we validated our methods for the polarizability and first hyperpolarizability. Our calculations for the polarizability differed from the literature by 3.37% to 6.56% while the first hyperpolarizability varied by 2.6.% to 17.06%. Our investigation into the the second hyperpolarizability revealed a strong dependence on the number of states for multiple basis sets. With methyl oxirane, we calculated the average polarizability to be 2.867 a.u., the parallel component of the first hyperpolarizability to be -240.5 a.u., and approximated the average second hyperpolarizability to be -1319 a.u. While future projects should continue to explore the inclusion of many more states, our preliminary results for methyl oxirane show that second harmonic generation studies may be particularly useful for experimental studies of the molecule.

# Table of Contents

# List of Figures

# List of Tables

# Chapter 1

# Introduction

In simplest terms, nonlinear optics (NLO) studies the responses and interactions between matter and high intensity optical fields. John Kerr performed the first observations of these nonlinear responses in 1875 when he examined electrically induced bifrengence in what is now known as the Kerr Effect[30;31]. After Kerr's observations, the field of NLO remained relatively untouched until its revival in the 20th century. In 1931, Maria Goeppert Mayer predicted two-photon absorption in her dissertation[21], a third order nonlinear effect. Experimental progress in nonlinear optics, however, remained scant until the advent of the laser, which provided experimentalists with a powerful optical source that could evoke these effects. Franken et al. took advantage of the new tool and demonstrated second harmonic generation in 1961[17]. In the following years, New and Ward discovered third harmonic generation[44]. Since these initial discoveries in NLO, the field has rapidly expanded and found use in several areas across physics. In particular, we shall discuss its application in laser systems, quantum optics, and imaging.

One of the uses of nonlinear optics is to produce green lasers. In these systems, an infrared laser is shone through nonlinear crystal to induce second harmonic generation, doubling the frequency to create a green beam[24;58;61]. More notably, nonlinear optics has become a core component in ultrashort laser pulse production[22;73]. One of the more important nonlinear

effects in ultrashort high harmonic generation (HHG)[34;52]. To achieve HHG, a crystal, liquid, or gas is illuminated the high intensity laser. The resultant laser field is a superposition of the initial laser frequency and harmonics (typically in the XUV range) several times higher than the initial[22]. Provided a pulsed laser is used, attosecond pulses are produced. It is important to note other methods involving consecutive second, third, and fourth harmonic generation processes have been proposed as well[52].

Beyond HHG, third order NLO has been applied to studies of various gas phase atoms and molecules. The Leone and Neumark groups have applied four-wave mixing (FWM) to studies of lifetimes in Rydberg states and traditionally inaccessible optical states. In their experiments, they applied a combination of XUV and NIR pulses to couple the excited electron to these states. By fitting the four-wave mixing signals, they measured the lifetimes of vibrational excitations[35], doubly excited states[60], and optically forbidden states[56]. The Shivaram group studied the electronic and librational dynamics of liquid nitrobenzene using similar four-wave mixing methods[65].

Beyond studying molecular dynamics through four-wave mixing, Shivaram has shown a method to probe the nonlinear coefficients directly[50]. Fundamentally, they align the molecules inside a gas cell using a pump pulse[51]. Following the pump pulse, three pulses are shone through the gas cell to initiate the nonlinear process. The FWM signal can then be measured in phase and amplitude against a reference pulse[50;51]. The FWM signal is directly proportional to the macroscopic lab-frame coefficient. This lab frame coefficient can then be related to the molecular frame coefficient through the appropriate rotations[50].

Quantum optics is another area that strongly relies on nonlinear optics. As the name would suggest, quantum optics investigates exotic, quantum states of light such as single photon states and pair photon states. Initially, these states were produced through nonlinear processes. The most prevalent of these processes is spontaneous parametric down conversion (SPDC)[10;26;38]. In SPDC, the input photons are annihilated and replaced with two entangled photons whose frequency adds to that of the inital photon[4]. For all intents and purposes,

SPDC creates and entangled pair of photons, but by measuring one of these photons, it becomes a single photon source[4]. For either application, SPDC has found a use in a variety of experiments from two-photon interference[27] to Bell Inequality tests[20].

Many biological compounds exhibit strong second order nonlinear responses[18;23;45]. These strong second order responses have leveraged to advance biophysical imaging[53]. Two of the more widely applied methods for biological imaging are two-photon excited fluorescence (TPEF)[3;74] and second harmonic imaging (SHI)[1;12]. In TPEF, dyes are applied to samples, these dyes are then excited through two-photon absorption. When the molecules relax to their ground state, they emit photons of a higher energy for detection[46]. The downside to this is that the dyes can be damaged by the laser. SHI, however, avoids this. Instead, SHI reflects the emitted second harmonics to be filtered and detected to reconstruct the image[67].

In the second chapter of this thesis, we will review the fundamental theory of nonlinear optics as well as the methods used to calculate the nonlinear coefficients. In chapter three, we will calculate the hyperpolarizabilities of the hydrogen fluoride molecule. We specifically look at hydrogen fluoride because it is a well studied molecule with several comparative calculations available in the literature. A suscessful calculation of the hyperpolarizabilities for hydrogen fluoride indicates our ability to compute the hyperpolarizabilities for other molecules.

Chapter four will review our calculations of the hyperpolarizabilities of methyl oxirane, a chiral molecule. Being a simple chiral molecule, methyl oxirane stands as a good candidate to study in terms of nonlinear effects. In particular, we want to examine the magnitude of the second order coefficients, as chiral molecules are known for their ability to exhibit second order effects[14] in isotropic solutions. Finally, in chapter five, we will review our results and provide directions for the continuation of this project.

# Chapter 2

# Theory

## 2.1 Theory of the (Hyper)polarizability

In electrodynamics, when we place a neutral body of charge in the presence of an electric field, the charges separate forming induced dipoles. If that electric field is oscillating, the entire body will have a time varying polarization density $\mathbf{P}(t)$ given by[29]

$$\mathbf{P}(t) = \epsilon_0 \int_{-\infty}^{\infty} \chi(\tau)\mathbf{E}(t-\tau)d\tau \tag{2.1}$$

Here, $\chi(t)$ is the time-domain electric susceptibility tensor and $\mathbf{E}(t)$ is the electric field. Moving to the frequency domain and applying the convolution theorem, we come to the constituency relationship

$$\mathbf{P}(\omega) = \epsilon_0 \chi(\omega)\mathbf{E}(\omega) \tag{2.2}$$

which shows that the amplitude of the polarization density will oscillate at the same frequencies as the external field with amplitudes proportional to the field strength.

When the electric field becomes sufficiently large, this relationship breaks down. In that case, we expand the polarization density[8] into a power series. Thus, the constituency

relationship is now

$$\mathbf{P}(\omega) = \epsilon_0 \left( \chi^{(1)}(\omega)\mathbf{E}(\omega) + \chi^{(2)}(\omega_\sigma)\mathbf{E}^2(\omega) + \chi^{(3)}(\omega_\sigma)\mathbf{E}^3(\omega) + \dots \right) \tag{2.3}$$

In this expansion, $\chi^{(n)}(\omega_\sigma)$ are the linear ($n = 1$) and non-linear ($n > 1$) susceptibilities. For each term in the expansion, we have used the following shorthand for the tensor products

$$\chi^{(n)}(\omega_\sigma)\mathbf{E}^n(\omega) = \chi^{(n)}_{ijk\dots l}(\omega_\sigma; \omega_\nu, \omega_\mu, \dots, \omega_\eta) E_j(\omega_\nu) E_k(\omega_\mu) \dots E_l(\omega_\eta) \tag{2.4}$$

We use the Einstein summation convention to sum over repeated indices. The indicies $i, j, k, l$ run over the cartesian directions, while $\nu, \mu, \eta$ run over the external field frequencies. The frequency $\omega_\sigma$ is equal to the sum of the external frequencies and is held fixed over the course of the summation. The result of this expansion is recognizing that the polarization density will oscillate at frequencies equal to various combinations of the external frequencies. This becomes more apparent in the time domain, where we would see a direct multiplication of sines and cosines (or complex exponentials). Table 2.1 provides examples of these frequency mixing processes for a monochromatic field with a d.c. offset.

**Table 2.1**: *Various nonlinear optical effects with their frequency inputs*[7;64]

| Input $\omega$ | Output $\omega$ | Name | Abbreviation |
|---|---|---|---|
| Second-Order Effects | | | |
| $(\omega, \omega)$ | $2\omega$ | Second Harmonic Generation | SHG |
| $(\omega, -\omega)$ | 0 | Optical Rectifcation | OR |
| $(\omega, 0)$ | $\omega$ | Electro-Optical Pockels Effect | EOPE |
| Third-Order Effects | | | |
| $(\omega, \omega, \omega)$ | $3\omega$ | Third Harmonic Generation | THG |
| $(\omega, \omega, -\omega)$ | $\omega$ | Degenerate Four Wave Mixing | DFWM |
| $(\omega, \omega, 0)$ | $2\omega$ | Electric Field Induced SHG | EFISH |
| $(\omega, -\omega, 0)$ | 0 | Electric Field Induced OR | EFOR |
| $(\omega, 0, 0)$ | $\omega$ | Electro-Optical Kerr Effect | EOKE |

Thus far, we have considered the perspective of bulk nonlinear optics, however, for a more fundamental approach, we must consider the individual molecules. Consider that a

general body of molecules or atoms will have some number denisty $\rho_N$. By dividing equation 2.3 by this number density, we retrieve an expression for the induced dipole $\mathbf{p}$ of one atom or molecule.

$$\begin{aligned}\mathbf{p}(\omega) &= \frac{\epsilon_0}{\rho_N}\chi^{(1)}(\omega)\mathbf{E}(\omega) + \frac{\epsilon_0}{\rho_N}\chi^{(2)}(\omega)_\sigma\mathbf{E}^2(\omega) + \frac{\epsilon_0}{\rho_N}\chi^{(3)}(\omega_\sigma)\mathbf{E}^3(\omega) + \dots \\ &= \alpha_X(\omega)\mathbf{E}(\omega) + \beta_X(\omega_\sigma)\mathbf{E}^2(\omega) + \gamma_X(\omega_\sigma)\mathbf{E}^3(\omega) + \dots \\ &= \alpha_T(\omega)\mathbf{E}(\omega) + \frac{1}{2!}\beta_T(\omega_\sigma)\mathbf{E}^2(\omega) + \frac{1}{3!}\gamma_T(\omega_\sigma)\mathbf{E}^3(\omega) + \dots\end{aligned} \tag{2.5}$$

We have regrouped our coefficients between lines two and three in equation 2.5 and defined new coefficients, the polarizability $\alpha$ and the first and second hyperpolarizabilities, $\beta$ and $\gamma$ respectively. The X and T subscripts refer to the convention being used. In the X convention, the power series from bulk nonlinear optics is directly carried over while the T convention uses a Taylor series[7;36;64]. The relation between susceptibilities and any order of hyperpolarizability $\alpha^{(n)}$ may be summarized as

$$\alpha_X^{(n)} = \frac{1}{n!}\alpha_T^{(n)} = \frac{\epsilon_0}{\rho_N}\chi^{(n)} \tag{2.6}$$

By considering the nonlinear effects on the molecular level, we can examine the contributions from various parts of molecular dynamics. In particular, the (hyper)polarizabilities are separated into electronic $\alpha_e^{(n)}$ and vibrational $\alpha_v^{(n)}$ contributions[5;7]. In some molecules, the vibrational contribution might outweigh the electronic. Although we will be focusing on the electronic contributions in this thesis, we shall briefly discuss the computation of vibrational contributions in the next section.

## 2.2 Computational Approaches

Several methods have been developed to calculate the electronic (hyper)polarizabilities of molecules. Generally, they are categorized into three groups: Sum Over States, (Pseudo-)Energy Derivatives, and Numerical Liouville Approaches. In this section we will look at select examples of these methods and their development. Importantly, all of these methods consider the same Hamiltonian:

$$H(t) = H_0 - \boldsymbol{\mu} \cdot \mathbf{E}(t) \tag{2.7}$$

where $H_0$ is the field free atomic or molecular Hamiltonian, $\boldsymbol{\mu}$ is the transition dipole operator, and $\mathbf{E}(t)$ is the oscillating electric field. The induced dipole is taken to be the expectation value of $\boldsymbol{\mu}$.

### 2.2.1 Sum Over States Methods

Sum Over States (SOS) methods are the result of applying time-dependent perturbation theory (TDPT) to solve the time-dependent Schrodinger equation (TDSE) with the Hamiltonian $H(t)$. Using TDPT, we solve for higher-order corrections to the induced dipole. By removing the electric field, we find an expression for the (hyper)polarizabilities in which all states that are not the initial state are summed over. The expressions for the polarizability and first hyperpolarizabilities (in T-convention) are

$$\alpha_{ij}(\omega) = \sum_n \frac{\langle 0|\mu_i|n\rangle\langle n|\mu_j|0\rangle}{\Omega_{n0} - \omega} + \frac{\langle 0|\mu_j|n\rangle\langle 0|\mu_i|n\rangle}{\Omega_{n0}^* + \omega} \tag{2.8}$$

$$\begin{aligned}\beta_{ijk}(\omega_\sigma;\omega_\nu,\omega_\mu) = \mathcal{P}\sum_{n,m}&\frac{\langle 0|\mu_i|n\rangle\langle n|\mu_j|m\rangle\langle m|\mu_k|0\rangle}{(\Omega_{n0}-\omega_\nu-\omega_\mu)(\Omega_{m0}-\omega_\mu)}\\ &+\frac{\langle 0|\mu_j|n\rangle\langle n|\mu_i|m\rangle\langle m|\mu_k|0\rangle}{(\Omega^*_{n0}+\omega_\nu)(\Omega_{m0}-\omega_\mu)}\\ &+\frac{\langle 0|\mu_j|n\rangle\langle n|\mu_k|m\rangle\langle m|\mu_i|0\rangle}{(\Omega^*_{n0}+\omega_\mu+\omega_\nu)(\Omega^*_{m0}+\omega_\mu)}\end{aligned} \tag{2.9}$$

In these expressions, $\Omega_{n0}$ is the difference between the $n$th excited state and the ground state energies, which in general is allowed to be complex with the addition of an imaginary relaxation factor. The operator $\mathcal{P}$ is the full permutation operator, which indicates the summation of all simultaneous permutations of the index pairs $(i,\nu)$ and $(j,\mu)$. For a full derivation and the third-order expression, we refer you to Boyd[9]. An alternative derivation is provided by Orr and Ward[48].

Another approach to develop a SOS form for the (hyper)polarizabilities comes from Response Theory[36;47]. Rather than applying traditional TDPT, we apply a unitary transformation to our initial state to handle the time evolution. Thus, our time evolving state is

$$|0(t)\rangle = e^{iS(t)}|0\rangle \tag{2.10}$$

where

$$S(t) = S_n\Lambda_n + S^*_n\Lambda^\dagger_n \tag{2.11}$$

Here, $\Lambda_n$ and its adjoint are excitation and deexcitation operators[36] and $S_n$ are time-dependent coefficients[47]. Rather than solving the TDSE, we use the relationship between the expectation value of $\Lambda$ and the expectation value of $\Lambda$ with the Hamiltonian. This equation simplifies to

$$\langle 0(t)|\Lambda|\dot{0}(t)\rangle + \langle\dot{0}(t)|\Lambda|0(t)\rangle = -i\langle 0(t)|\left[\Lambda, H(t)\right]|0(t)\rangle \tag{2.12}$$

Expanding $S_n$ perturbatively leads to solutions that provide response functions for any operator. Applying the response function to the $\mu$ results in formulae very similar to those

derived in Boyd. The primary difference is that $\langle n|\mu_j|m\rangle$ in the numerators is replaced with $\langle m|\mu_j|n\rangle - \delta_{mn}\langle 0|\mu_j|0\rangle$ in second-order and higher[36].

SOS calculations have developed a further use, as the first method to calculate the vibrational contributions evolved from them. Bishop and Kitman developed a perturbative approach to calculating the vibrational contributions in an SOS expression[6]. Through their derivation, they show that electric and mechanical anharmonicity influences these vibrational components. For a more thorough derivation and discussion, we refer you to Bishop and Kitman's original paper[6].

Despite the straightforward formulae, the SOS approach is impractical for ab initio calculations with molecules with more than a few atoms[7]. This restriction stems from the need of many highly electron-correlated wavefunctions for the calculations of molecular properties[7]. To avoid this on the semi-empirical level, the sum may be truncated, introducing obvious numerical deviations from other methods. Additionally, this method is incapable of directly handling on-resonance calculations. In the Boyd expressions, if we do not include the imaginary relaxation term to the molecular energies, the (hyper)polarizabilities approach infinity at resonances. Furthermore, often times this relaxation term will also be semi-empirical in nature. Through the response theory, the resonant calculations may be considered through residue analysis[7].

### 2.2.2 (Pseudo)Energy Derivative Methods

Cohen and Roothan first introduced the energy derivative method with their Finite Field (FF) approach. In the original FF method, they used a static field to calculate the polarizability[37]. Despite being presented for first-order calculations, it was developed and applied to the hyperpolarizabilities[39]. The FF method, however, is only applicable to the static (hyper)polarizabilities.

Sekino and Bartlett advanced the energy derivative method by applying Time-dependent Hartree-Fock (TDHF) to the problem of a molecule in an oscillating field[63]. This gave a

way to calculate the dynamic (hyper)polarizabilities for molecules but failed to properly account for electron correlation effects. Rice and company amended this by applying second order Møller Plesset Perturbation Theory[25] (MP2). However, instead of using the energy or induced dipole of the molecule, they used the pseudo-energy[57].

$$W = \langle \psi | H(t) - i\partial_t | \psi \rangle \tag{2.13}$$

This pseudo-energy (also called quasi-energy) is also used in the Floquet Theory approach. In Floquet Theory, we aim to find an exact solution to the TDSE with an oscillating field by means of a Fourier expansion of the wavefunction and the polarization. Using the nonlinear constituency relations presented in equations 2.3 and 2.5, it is plain to see the relation of the susceptibilities/(hyper)polarizabilities as a polarization derivative. Leveraging the Hellman-Feynman theorem, this converts to a pseudo-energy derivative. A full derivation of this method is presented by Shtoff et al.[66]

The practicality of the derivative methods is countered by the sensitivity inherent in numerical derivatives. It is well understood that for numerical derivatives, care must be taken to choose the appropriate electric field values to minimize these sensitivities[39]. However, numerical derivatives only apply to the FF approach. The complex nature of the orbitals requires the use of analytical expressions for the derivatives from TDHF or MP2[64]. This, however, introduces two different issues. First, it's known that TDHF and MP2 may miss important electron correlation effects[7;25;63]. Second, when performing a calculation on resonance, the resonance will be improperly located due to excited state energies which will be inaccurate[25].

### 2.2.3 Numerical Liouville Approach

The Numerical Liouville Approach was developed and introduced by Nakano and Yamaguchi as a way to compute intensity dependent susceptibilities for any order[41;42]. First, static

calculations are performed to generate the excited state energies and dipole matrix elements for the molecule of interest. These are then used in the Liouville equation

$$\rho(t) = -i\,[H(t), \rho(t)] \tag{2.14}$$

to determine the time evolution of the system $\rho(t)$. The induced dipole is then calculated as

$$\mathbf{p}(t) = Tr[\boldsymbol{\mu}\rho(t)] \tag{2.15}$$

The Fourier transform of both the field and the induced dipole are taken. The intensity dependent (hyper)polarizability is then calculated as[41]

$$\alpha^{(n)}_{g,ijk\ldots l}(\omega_\sigma) = \frac{p_i(\omega_\sigma)}{E_j(\omega_\nu)E_k(\omega_\mu)\ldots E_l(\omega_\eta)} \tag{2.16}$$

In the limit of a field at the early in the nonlinear regime, $\alpha^{(n)}_g$ reduces to the perturbative form $\alpha^{(n)}$[42]. In this approach, however, there is the risk of numerical noise corrupting the results from this calculation. To offset this, we consider another approach involving multiple repeated solutions to the Liouville equation at various electric field strengths.

If we calculate the polarization along a grid of electric field points, which ranges from $-E_0$ to $E_0$, we can use polynomial regression to determine the hyperpolarizabilities. For simplicity, we consider an electric field polarized along one of the cartesian axes to use in our Hamiltonian. After solving equation 2.14 along this grid, we assemble our induced dipoles and electric field points into the vectors $\vec{p}_i(n\omega)$ and $\vec{E}_j(n)$, where

$$\vec{p}_i(n\omega) = \begin{pmatrix} p_{i,1}(n\omega) \\ p_{i,2}(n\omega) \\ p_{i,3}(n\omega) \\ \vdots \\ p_{i,n_E}(n\omega) \end{pmatrix} \tag{2.17}$$

$$\vec{E}_j(n) = \begin{pmatrix} E^n_{j,1}(\omega) \\ E^n_{j,1}(\omega) \\ E^n_{j,1}(\omega) \\ \vdots \\ E^n_{j,n_E}(\omega) \end{pmatrix} \tag{2.18}$$

We have taken the maximum number of electric field points to be $n_E$. We then represent the (non)linear constituency relations as a general vector equation for all $n_E$ points. The form of this equation is fundamentally identical to the constituency relations, except the polarization components are replaced with our new vectors.

$$\vec{p}_i(n\omega) = \alpha^{(n)}_{ijj\ldots j}(n\omega)\vec{E}_j(n) \tag{2.19}$$

We solve the vector constituency equation 2.19 for the general (hyper)polarizability by using least squares polynomial fitting[19]. Thus, we express the (hyper)polarizabilities as

$$\alpha^{(n)}_{ijj\ldots j}(n\omega) = \frac{\vec{E}_j(n)^\dagger \vec{p}_i(n\omega)}{|\vec{E}_j(n)|} \tag{2.20}$$

In the case of $n = 1$, we calculate the linear polarizability, and when $n > 1$ we calculate the hyperpolarizabilities. Additionally, in the case of $n_E = 1$ this general method reduces to the NLA introduced by Nakano. One benefit of this method is that it may be readily expanded to account for multiple orders influencing the polarization at a particular frequency. To do this, we would use multiple polynomial regression, expanding our vector of electric field points into matrix with each each $E_j(n\omega)$ being its own variable. For our calculations in future chapters, we will use this general method to solve for the specific cases of the dynamic polarizability and the hyperoplarizabilities for SHG and THG.

Similar to the numerical energy derivative methods, the choice in the electric field will greatly influence the results of calculations. With too weak of a field, the extended power

series is unneeded to describe the induced dipole, and with too strong of a field, the power series breaks down and no longer describes the induced dipole. Furthermore, on resonance calculations of the hyperpolarizabilities are well handled by the NLA, but may have increased field dependence compared to off-resonance calculations[42]. Finally, we must consider that although Nakano[40] and company as well as Bishop[7] claim that few states are needed for calculations, this may change depending on the molecular properties inherent in the molecule's structure.

## 2.3 Symmetry Properties of NLO Coefficients

When calculating the nonlinear coefficients, it is important to consider how symmetry affects the (hyper)polarizability or nonlinear susceptibilities. Depending on the symmetry of a molecule or atom, certain orders of nonlinearity may not occur. In centrosymmetric molecules (and all atoms), for instance, even-order nonlinear effects are forbidden. This originates from the violation of inversion symmetry that occurs in the second-order, that is the induced dipole in all orders must change sign when the external field changes sign. Because even-order effects result will have the field raised to an even power, the sign of the nonlinear contribution is entirely dependent upon the hyperpolarizability, thus violating inversion symmetry.

The structure of the hyperpolarizability tensors is also reliant upon the symmetry of the molecule. The number of independent elements will depend on the symmetry group of the molecule. For further discussion, we refer you to Boyd[8]. Although Boyd discusses in terms of the nonlinear susceptibilities, we readily extend them using the relation between $\chi^{(n)}$ and $\alpha^{(n)}$ in equation 2.6.

Another symmetry property of the hyperpolarizabilities comes from a matter of convention, but is important to note, nonetheless. For simplicity, we continue to work in terms of the second-order coefficient. Consider, then, the nonlinear induced dipole contribution in its fully expanded form.

$$p_i^{(2)} = \beta_{ijk}(\omega_\sigma; \omega_\nu, \omega_\mu) E_j(\omega_\nu) E_k(\omega_\mu) \tag{2.21}$$

In this expression, we have used arbitrary indices for our input fields. In actual calculations, it does not matter which fields are the $i$th field with the $\nu$th frequency. Thus, we should be able to simultaneously permute the frequencies and the cartesian indices and resolve the same hyperpolarizability. This is referred to as intrinsic permutation symmetry. In the case of a lossless medium, we expand this into full permutation symmetry. In full permutation symmetry, we may also permute the frequency and index of induced dipole, however a sign change is implemented on the frequencies depending on the position they move to.

Finally, the last symmetry to consider is Kleinman's Symmetry. When the frequency of the incoming optical waves are significantly less than the frequency of the first resonance, the frequency dependence may be neglected. Thus, rather than a simultaneous permutation of frequencies and cartesian indices, only the cartesian indices need be permuted to resolve the same hyperpolarizability.

## 2.4 The Basis Set Problem

Throughout the literature, it is well established that the largest obstacle in calculating accurate hyperpolarizabilities is the choice in basis[7;54;64;75], i.e. the set of functions used to represent the electronic wavefunction. These basis sets rapidly increase in size[7] with functions meant to more accurately describe the polarization of the molecule and the wavefunction far from the nuclei being added to the basis sets[54;75]. These functions are referred to as polarization and diffuse functions respectively. Diffuse functions in particular have a strong influence on the second hyperpolarizability[37]. The downside of such large basis sets is the computational cost. This led to the development of basis sets and design philosophies for basis sets to calculate the hyperpolarizabilities.

One of these specially designed basis sets came from Pluta and Sadlej as an evolution of their Pol basis set, which they called the HyPol basis[54]. In particular, they focus on the development of the basis for first and second row atoms (as well as H and He). In general, they start with their Pol basis set, which is of the form $[nsmpld/NsMpLd]$ where $n, m, l$ correspond to the number of uncontracted functions and $N, L, M$ correspond to the contracted functions for that orbital type. The functions of the core and valence orbitals are unaltered, but the most diffuse polarization functions are decontracted. The exponents of the diffuse polarization are then reused when adding higher order polarization functions. These polarization functions take the form of orbitals with the next highest angular momentum. For a more extensive discussion, we refer you to Pluta and Sadlej's paper[54].

Zuev and Nefdiev developed their own rules for basis set design tailored for the calculation of the first hyperpolarizability[75]. Additionally, they design this basis with the goal of optimizing the basis set regardless of how the functions are contracted. For the full discussion we refer you to their paper[75], however we will sumamrize the general procedure here. While they develop rules for the addition of diffuse $s$ and $p$ functions, more notable is their development for the addition of the first $d$ polarization function. To determine these exponents, they minimize the Hartree-Fock atomic orbital energy with respect to the $1d$ function in the presence of an electric field. The higher $d$ orbital function exponents are developed from known methods. The $f$ orbital functions are then built using the exponents of the $d$ orbital functions. In general, the resulting basis set family is of the form $[11s7pNdMf]$ and tailored to calculations featuring electric field responses.

# Chapter 3

# The Hyperpolarizabilities of Hydrogen Fluoride

## 3.1 History of Calculations

Over the years, significant effort has been put into calculating the optical coefficients of hydrogen fluoride. Despite being a relatively simple molecule, HF garnered a lot of attention due to divergence between theoretical and experimental results. This lead to the continual development of basis sets and approaches that tried to account for missing effects. Table 3.1 compiles the results of several calculations performed over the years, which we will consider in this section. It is important to note that most computations limit themselves to the second-order, likely due to the the difficulty in converging the third-order coefficients.

Sekino and Bartlett[63] presented the first dynamic calculations for HF when they introduced the TDHF Energy Derivative approach to (hyper)polarizabilities. In their calculations, they applied three basis sets. The first two bases are the double-zeta Dunning basis set without and with polarization functions. The third basis set they use is one of their own creation, a $[6s5p4d2f/5s3p]$ basis. Sekino and Bartlett themselves (as well as Bishop[7]) note that their basis sets are too small to give satisfactory results.

**Table 3.1**: *A compilation of calculations of the optical properties of hydrogen fluoride at* $\omega = 0.0656$ *a.u. from various authors. Bolded values are isotropic averages of the (hyper)polarizabilities, and unbolded values are solely along the z-axis. For basis resented as* $[nsmpld.../asbp...]$*, the first set of functions corresponds to F and the second to H. Aiga's P1 basis corresponds to* $[12s8p5d4f/8s6p3d]$*, and P2 corresponds to* $[14s10p6d4f/9s8p3d]$*. Kobayashi et al's mPOL basis corresponds to* $[5s3p2d/3s2p]$*, and the mHyPOL corresponds to* $[5s3p3d2f/3s3p3d]$*. Using these values, we can judge the quality of our calculations in the following sections.*

| Author | Method | Basis | $\mu_z$ | $\alpha(\omega)$ | $\beta^{SHG}(2\omega)$ | $\gamma^{THG}(3\omega)$ |
|---|---|---|---|---|---|---|
| $\omega = 0$ a.u. | | | | | | |
| Sekino and Bartlett[63] | TDHF Energy Derivative | DZ | 0.936 | 4.002 | -17.589 | 126.31 |
| | | DZP | 0.807 | 4.294 | -14.466 | 102.98 |
| | | $[6s5p4d2f/5s3p]$ | 0.757 | 5.764 | -8.543 | 275.13 |
| Aiga[2] | TDHF Response Theory | P1 | 0.756141 | 5.7540 | -8.4579 | |
| | | P2 | 0.756200 | 5.5741 | -8.4342 | |
| Rozyczko and Bartlett[59] | EOM-CC SOS | cc-pVTZ | | | -12.87 | 306 |
| | | aug-cc-pVTZ | | | -11.71 | 311 |
| | | d-aug-cc-pVTZ | | | -9.87 | 369 |
| | | t-aug-cc-pVTZ | | | -9.84 | 378 |
| Kobayashi et al.[32] | QED-MP2 | mPOL | 0.70841 | 6.3902 | -8.9184 | |
| | | mHyPOL | 0.70629 | 6.4346 | -9.1979 | |
| | | t-aug-cc-pVTZ | 0.70880 | 6.3830 | -8.8328 | |
| $\omega = 0.0656$ a.u. | | | | | | |
| Sekino and Bartlett[63] | TDHF Energy Derivative | DZ | 0.936 | 4.039 | -18.739 | 155.47 |
| | | DZP | 0.807 | 4.327 | -15.367 | 125.66 |
| | | $[6s5p4d2f/5s3p]$ | 0.757 | 5.808 | -9.194 | 336.19 |
| Aiga[2] | TDHF Response Theory | P1 | 0.756141 | | -9.1219 | |
| | | P2 | 0.756200 | | -9.0968 | |
| Rozyczko and Bartlett[59] | EOM-CC SOS | cc-pVTZ | | | **-9.04 ± 0.5** | **462 ± 40** |
| | | aug-cc-pVTZ | | | **-8.04 ± 0.5** | **598 ± 40** |
| | | d-aug-cc-pVTZ | | | **-8.52 ± 0.5** | **669 ± 40** |
| | | t-aug-cc-pVTZ | | | **-8.70 ± 0.5** | **711 ± 40** |
| Kobayashi et al.[32] | QED-MP2 | mPOL | 0.70841 | 6.4434 | -9.7443 | |
| | | mHyPOL | 0.70629 | 6.4888 | -9.9727 | |
| | | t-aug-cc-pVTZ | 0.70880 | 6.4369 | -9.6006 | |
| Dudley and Ward[15;59] | Experiment | N/A | | | **11± 1** | **840± 120** |

Aiga et al.[2] approached the HF problem from a different angle, using response theory under TDHF rather than the energy derivative approach of Sekino et al. Additionally, they apply two larger basis sets which they developed from previous basis sets. In short, the P1 basis was produced through a repeated contraction and augmentation of a $(13s8p/8s)$ basis with the additional $d$ function on H and $f$ functions on F being generated as even-tempered functions. The P2 basis is built from an initial $(16s10p/10s)$ basis which is also contracted and augmented using their proposed "smooth-tempered basis" calculations. For full discussion, we refer to their paper[2] Their results, while showing some agreement with Sekino, are also insufficient, and only approach the Hartree-Fock limit while both methods only include correlation at the TDHF level.

Rozyczko and Bartlett[59] approached the problem with a much more robust method, applying the equation-of-motion coupled-cluster singles, doubles (EOM-CCSD) level of theory to account for dynamic correlations in their computations. They worked with several augmented Dunning basis sets, but we show the results for only a few. One downside to their calculations is that they only present results for the isotropic averages of the optical coefficients for particular effects. Their results, however, still do not resolve the discrepancy between theory and experiment, though they explore several reasons for the discrepancy, such as the inclusion of triple excitations, vibrational contributions, and orbital relaxation. The exclusion of orbital relaxation, they note, would lead to an increase of about 0.4 a.u. and 10 a.u. to their results for the first and second hyperpolarizabilities respectively.

Kobayashi et al.[32] performed their calculations using both the TDHF method and QED-MP2 method with three basis sets. Table 3.1 only reports the QED-MP2 results, but it is important to note that the magnitudes were larger for all basis sets when compared to the TDHF results. Despite the increase in magnitude for $\beta$, when compared to the experimental results, there was still a significant discrepancy.

Dudley and Ward[15] are the most commonly cited authors for a comparison against experimental results for the hyperpolarizability of HF. Their results, however, are not for the

hyperpolarizabilities directly. Instead, they measure $\chi_{||}^{(2)}$ and $\chi_{||}^{(3)}$, which are related to the first and second hyperpolarizabilities by a factor of 1/2 and 1/6 respectively[15]. We have made use of Rozyczko and Bartlett's conversion reported in their results[59] for simplicity. Additionally, their measurment of $\chi_{||}^{(3)}$ corresponds to EFISH rather than THG. Reviewing Rozyczko and Bartlett, however, shows that although not an exact comparison, the values for THG and EFISH should be within 100 a.u. of each other.

Despite the difficulties encountered in calculating the hyperpolarizabilities for this molecule, the theoretical computations have managed relatively consistent results. This consistency makes for a good ruler to measure our code against. If the calculations performed with our code are in reasonable agreement with the literature, we are in a good position to extend our analysis to other molecules. In particular, measuring against the literature of hyperpolarizabilities for HF will give us an idea of where our calculations stand as preliminary caclulations for the hyperpolarizabilities of methyl oxirane.

## 3.2 Numerical Liouville Calculations for HF

### 3.2.1 Computational Details

To calculate the energy levels and dipole matrix elements, we used the EOM-CCSD program[33] in Molpro[70–72] using several basis sets using an internuclear distance of $r = 0.92$Å aligned along the z-axis. Initially, we considered the cc-pVTZ, cc-pVQZ bases with their singly augmented counterparts as well as Pluta and Sadlej's HyPol basis[54]. For all test calculations, we used an electric field polarized along the z-axis with a frequency of $\omega = 0.0656$ a.u. To solve the Liouville equation, we used SciPy's differential equation solver with the eighth-order Runge-Kutta method DOP853[69].

To measure the effectiveness of our basis sets against each other, we first considered the convergence of the optical coefficients with respect to the number of included states. For this calculation, we set the magnitude of the electric field to $|E_0| = 10^{-3}$ a.u. Fig 3.1 depicts the

results of these calculations for the polarizability component $\alpha_{zz}$. In the figure, we see cc-pVTZ and cc-pVQZ bais sets converge to values of 5.1186 a.u. and 5.4753 a.u. respectively. In the case of the cc-pVTZ basis, a 5-state system converges us to 93.99% of the final value, but to be converged up to the second decimal place, we require 14 states. The cc-pVQZ basis converges to the first decimal place at 8 states with the second and third decimal convergent at 15 states. When compared to the literature, these values are already in rough agreement with Sekino and Bartlett's values from Table 3.1.

Examining the other basis sets, we see a more consistent and repeated staircase pattern in their convergence. By the final steps, each basis set is seemingly converged to at least the first or second decimal place. Without examining the inclusion of further states, we cannot make any claims to convergence. However, comparing the values of the full 17 state system, all except the HyPol basis produce values in agreement with the literature and within 0.4 a.u. of each other. The aug-cc-pVTZ basis in particular exhibits excellent agreement with our calculations with the cc-pVQZ.

Fig 3.2 shows the results of the state convergence test for the first hyperpolarizability component $\beta_{zzz}$. Across all basis sets, we see large jumps in the calculated values. The cc-pVTZ and cc-pVQZ bases are the first to approach convergence. While at a 10-state system the influence of more states severely decreases, it is not until a 14-state system that we see convergece to the first decimal place. The cc-pVQZ basis exhibits similar behavior, remaining within 2.12% of the converged value starting at 8 states with the 15-state system converging to two decimal places. These final values for the cc-pVTZ and cc-pVQZ bases are notably smaller in magnitude than the literature, which may be the result of improper electric field strength or number of regression points.

The other basis sets continue to produce several small stable regions before making jumps in their values. By the 16 states, they all remain within 0.02 a.u. of their final value. The most notable case from these remaining basis sets is the HyPol basis, which calculates $\beta_{zzz} = -9.02$ at 17 states, which agrees with the literature. Again, we encounter that because

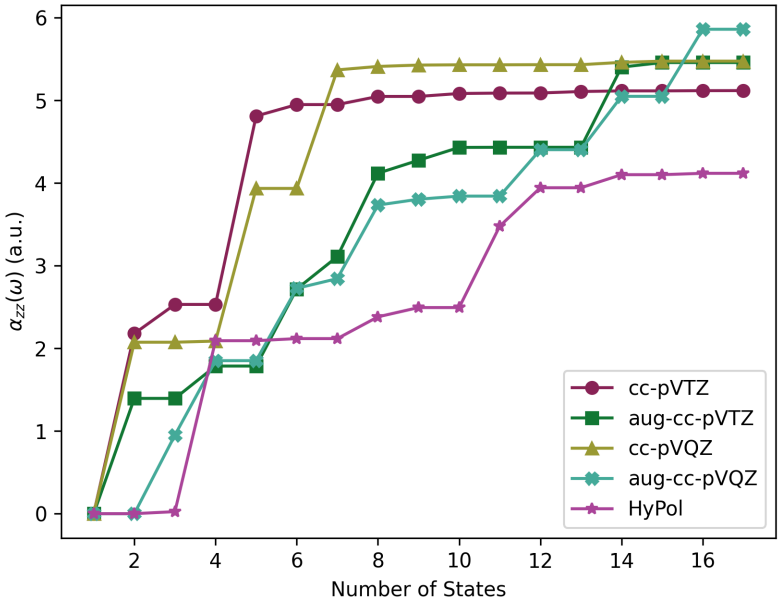


**Figure 3.1**: *Plot of the polarizability of HF with respect to the number of states used in the calculations. The cc-pVTZ basis begins to converge at 5 states, where it reaches 93.99% of the final value. At 10 states, convergence improves to 99.41%. The cc-pVQZ basis begins converging at 7 states reaching 98.06% of the final value. At 10 states, convergence improves to 99.19%. Other bases reach similar convergences over many fewer states, thus we can less confidently claim they are converged rather than at temporary plateau. The cc-pVTZ and cc-pVQZ basis closely match Sekino and Bartlett in the literature with a value of 5.0886 and 5.4308 a.u. respectively.*

of the frequent jumps we cannot make a claim to any convergence.

Finally, we consider Fig 3.3, which shows the results of basis set and state convergence for $\gamma_{zzzz}$. First to note is that the end points for the third-order results are the most varying, which makes sense. Given the volatility that comes with a third-order nonlinearity, such a large disagreement between basis sets is not entirely surprising. A bit more surprising is the order of magnitude difference between the final values we have calculated and the ones in the literature. Additionally, the cc-pVTZ basis reaches the most stable value only varying by 2.88% of the final value, 1505 a.u. The cc-pVTZ basis is also important to note. Starting at 5 states, it is monotonically increasing. The value calculated from the 17-state system in the cc-pVTZ basis is also of the same order of magnitude as in the literature, but the

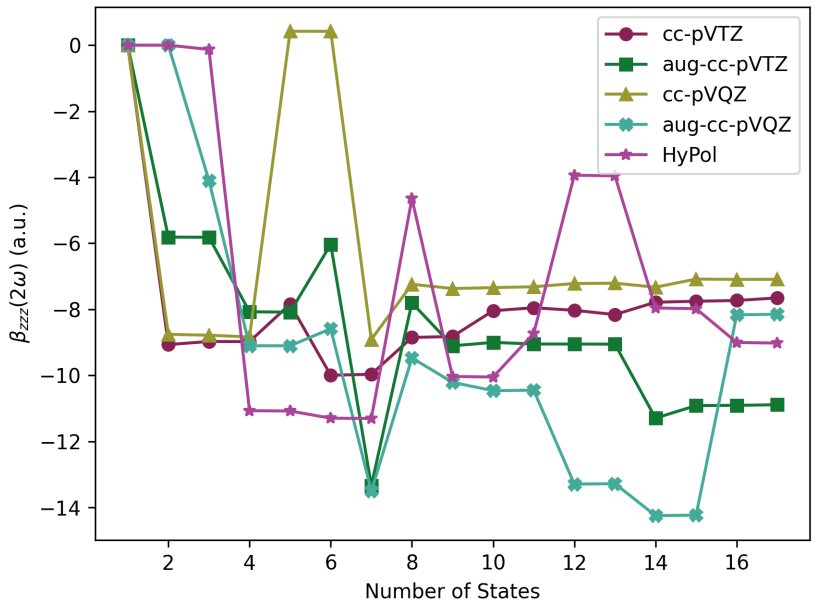


**Figure 3.2**: *Plot of the first hyperpolarizability of HF with respect to the number of states used in the calculations. The cc-pVTZ basis begins to converge by 10 states, however it takes until state 14 to converge to stablize the first decimal place. The cc-pVQZ basis begins to converge by 8 states, but does not converge two to decimal places until 15 states. Similar to the polarizability, the other basis sets reach similar convergences along short plateaus, but we cannot confidently claim that they are not at a plateau. The cc-pVTZ and cc-pVQZ basis sets match closest to Rozyczko and Bartlett's values, however they are still smaller in magnitude at -7.7 and -7.09 a.u. respectively.*

opposite sign.

Given the cc-pVTZ's promise with the polarizability and first hyperpolarizability, we have decided to investigate the convergence of this basis set if we extend the system to include up to 40 states. Fig 3.4 is the results of extending our calculations of the second hyperpolarizability to 40 states. As we anticipated, the second hyperpolarizability continued to increase with several states. By 30 states, it has started to oscillate from 329 a.u. to 507 a.u. Both of these numbers are comparable to the results Rozyczko and Bartlett calculated, as presented in Table 3.1.

We intend to continue exploring the influence the number of states has on this system, however for this thesis, we will utilize the cc-pVQZ basis. This basis converged the most

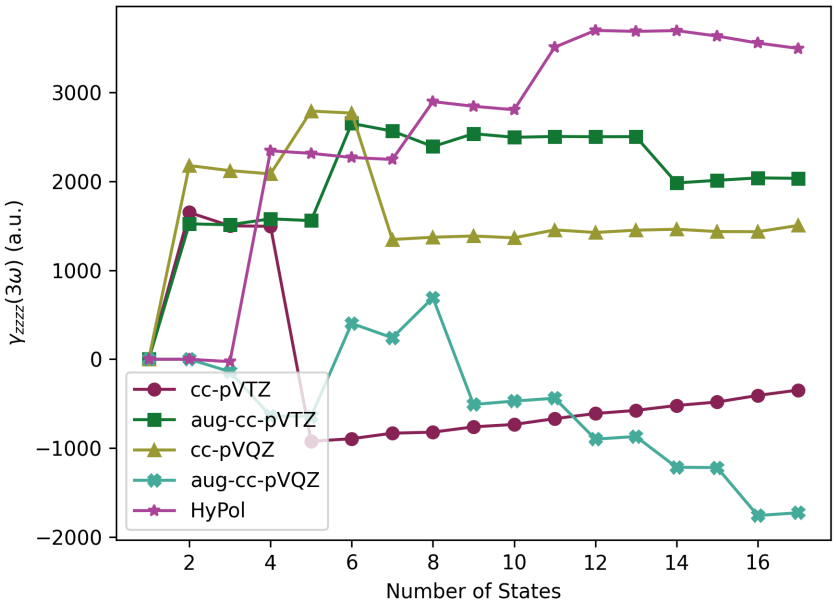


**Figure 3.3**: *Plot of the second hyperpolarizability of HF with respect to the number of states used in the calculations. By 10 states, the cc-pVQZ basis begins converging to a stable numeral in the hundreds position. Remarkably, the value it converges to is an order of magnitude larger than anything in the literature. The cc-pVTZ basis, although not converged, is monotonically increasing at the 5 state mark. The other bases exhibit similar convergence on the plateaus, but we cannot claim whether these are plateaus or convergence.*

readily across all orders, but the exact reason why is currently unknown. Additionally, in first and second the results thus far produced seem reasonable. We will use a 10-state system to model HF as the convergence at that point is sufficient for our purposes.

### 3.2.2 Determining Computational Parameters

Next, we consider the effect the electric field strength has on the (hyper)polarizabilities. As previously mentioned, we continue with the 10-state system, and we will continue to use a single regression point. The electric field is a particularly important parameter, at too low of a field strength, we fail to see accurate behavior for the (hyper)polarizabilities, but at too high of a field strength we risk including higher-order terms or saturating the results. Fig 3.5 shows the results calculated with the cc-pVQZ basis. The polarizability is not largely

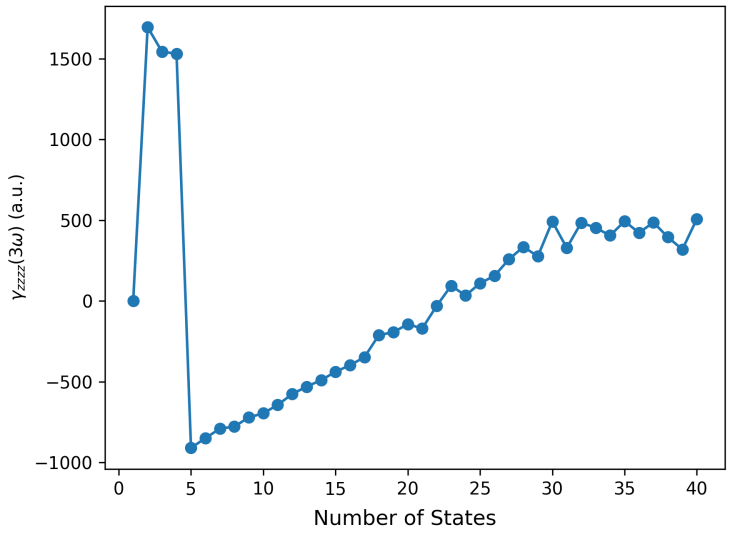


**Figure 3.4**: *Plot of the second hyperpolarizability as calculated with the cc-pVTZ basis up to a total of 40 states included. The value of the hyperpolarizability continues to slowly increase until around the 30 state mark. By 30 states, it has started to oscillate between approximately 300 and 500 a.u. These values are in agreement with the literature, in particular it is good to compare with Rozyczko and Bartlett's cc-pVTZ value.*

influenced by changing the strength of the field; The first and second polarizabilities, however are significantly influenced. Ultimately, this leads us to reduce the electric field strength to $|E_0| = 4 \times 10^{-4}$ a.u. to avoid potential saturation that might occur with stronger fields. It is important to note that this is also close to the value used by Nakano et al.[42]

Finally, we consider the effect of using multiple regression points as opposed to just one. Using the converged parameters from the previous tests, we evaluated the (hyper)polarizabilities using up to 20 regression points in the previously discussed standard polynomial regression procedure. To exemplify our methodology, we consider Fig 3.6 as an example of the results of our fitting procedure. In this figure, we have fit five $(E_0, p_i(n\omega))$ points to the appropriate polynomial for each order. Examining by eye, we see that in general our fits sufficiently describe the polynomials. Repeating these calculations over several differing numbers of points, we see how each coefficient varies with the number of points.

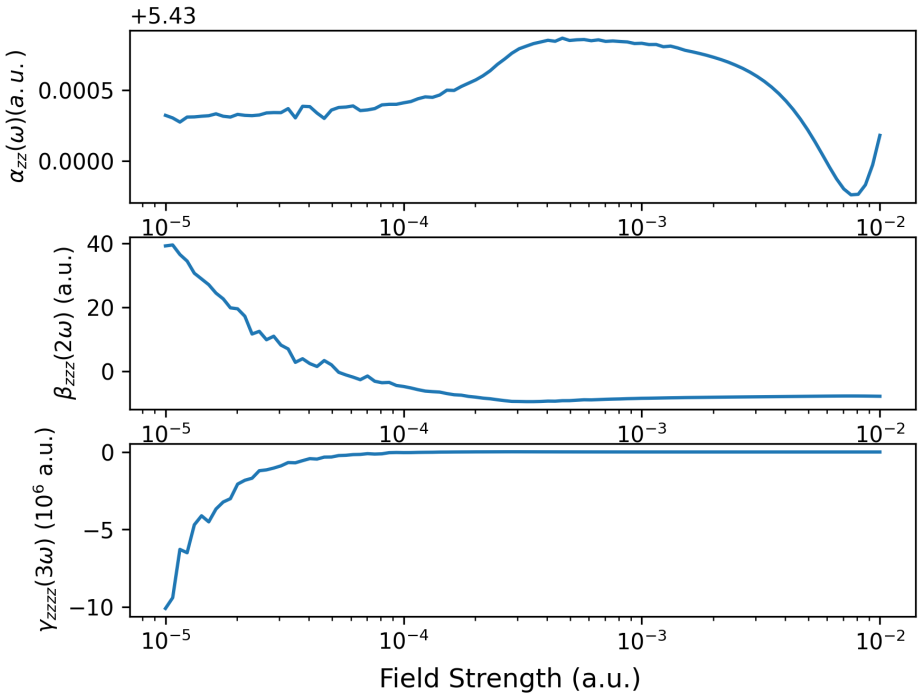


**Figure 3.5**: *Plots of the polarizability (top), first (middle), and second (bottom) hyperpolarizabilities of HF with respect to the electric field strength using the cc-pVQZ basis. A region of stability for all parameters forms in the region* $10^{-4} \lesssim E_0 \lesssim 10^{-3}$. *Additionally, the first hyperpolarizabilities appears saturated.*

These results are found in Fig 3.7 Again, the linear term is not influenced much, but the quadratic and cubic terms are influenced much more. No real point of convergence is reached, however, thus when evaluating these, we will compare the application of several different numbers of regression points.

### 3.2.3 Results and Discussion

Table 3.2.3 shows the results of our computations for the static and dynamic calculations of the (hyper)polarizabilities for HF. For the case of our static calculations, we see that our polarizability is in agreement with the literature. The first and second hyperpolarizabilities, however, do not agree with the literature. Both are multiple orders of magnitude larger than the literature reports. The reason for this disagreement stems from our method of

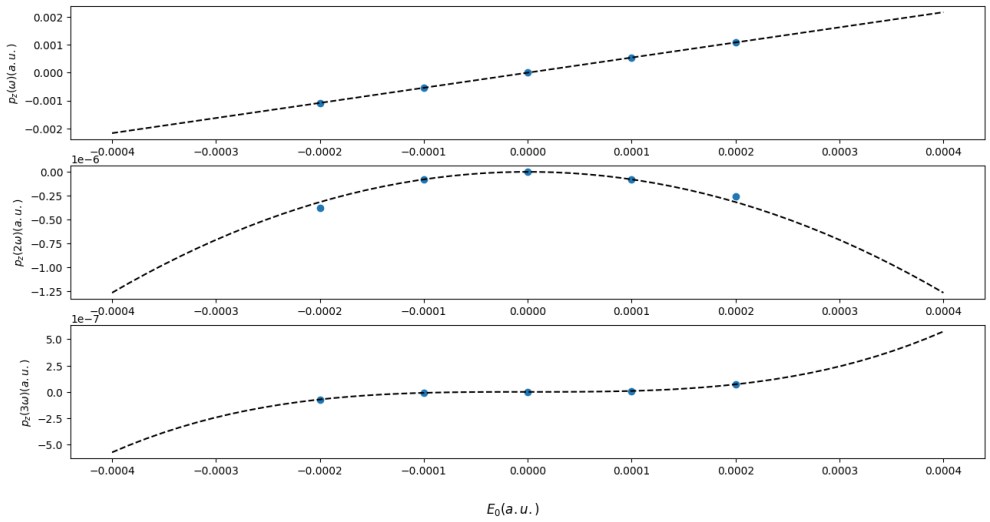


**Figure 3.6**: *Plots of five* $(E_0, p_i(n\omega))$ *points for HF ranging from* $-E_0$ *to* $E_0$ *used for fitting the nth order polynomials for each order. The coefficients calculated for these fits show fair agreement with the points used for the fits.*

calculation. In the case of $\omega = 0$, both the linear and nonlinear terms will contribute to $p_z(0)$, thus fitting each term separately is insufficient for terms beyond the dominant, linear term.

Looking at our results calculated at the ruby laser frequency, we once again see fair agreement in the polarizability. While Aiga does not calculate the dynamic polarizability, the static polarizability can act as a sufficient approximation. We know the polarizability should not drastically change far from resonant frequencies. When comparing our dynamic results to their static ones, we find a 6.56% difference for their calculation with the P1 basis. For the P2 basis, we find a percent difference of 3.37%. These are interesting results. Beyond the fact we are comparing to a static value, Aiga's results are recognized as approaching the Hartree-Fock limit[2]. This is an odd result, as we are using a post-Hartree Fock method to calculate our molecular properties.

We shall compare our dynamic first hyperpolarizability calculations against Rozyczko and Bartlett's, as they have also made use of EOM-CCSD in their calculations. For the case of one regression point, we find that compared to their highest value, there is a 5.38%

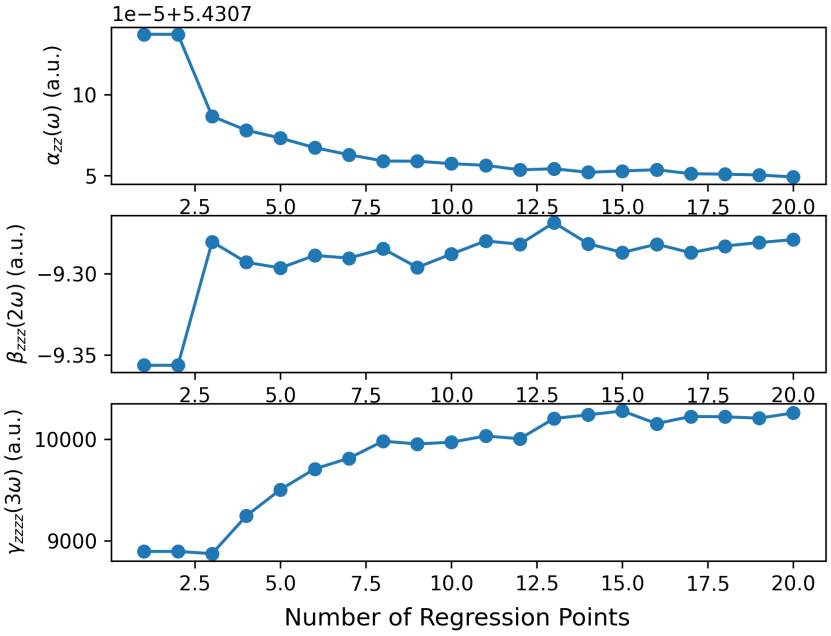


**Figure 3.7**: *Plots examining the effect of increasing the number of regression points on calculations of the (hyper)polarizabilities. The polarizability is largely unaffected by increasing the number of regression points, only changing by the fifth decimal place. After the initial jump in the first hyperpolarizability, the value oscillates from -9.29 a.u. to -9.27 a.u. The second hyperoplarizability converges to the tens place by 17 regression points, the final value reached is 1025 a.u.*

difference. Against their lowest value, the percent difference between our results is 17.06%. If we compare against our results calculated with three regression points, the percent difference ranges from 14.32% to 2.62%. If we instead consider our results in terms of the uncertainty estimated by Rozyczko and Bartlett, our results remain within reason. To be precise, our results fall well within the $0.5a.u.$ uncertainty applied to their result with the highest magnitude.

Our agreement with Rozyczko and Bartlett (as well as other theory), however, means we disagree with experiment. In fact, when considering the $1a.u.$ uncertainty on the results from Dudley and Ward, our results still fall outside of the experimental measurements. Instead, our calculations differ from experiment by $1.5a.u.$ to $1.8a.u.$ Although this is unfortunate, it is not unexpected. Recall, there is notorious disagreement between theory and experiment with

**Table 3.2**: *Results for the (hyper)polarizabilities of HF in atomic units at $\omega = 0$ and $\omega = 0.0656$ a.u. calculated using the traditional NLA ($n_E = 1$) and NLA with regression ($n_E = 3$). Select theoretical and experimental results from the literature are presented as well for comparison.*

| $\omega$ (a.u.) | $\alpha_{zz}(\omega)$ (a.u.) | $\beta^{SHG}_{zzz}(2\omega)$ (a.u.) | $\gamma^{THG}_{zzzz}(3\omega)$ (a.u.) |
|---|---|---|---|
| $n_E = 1$ | | | |
| 0 | 5.3889 | -1347 | $3.368\times10^7$ |
| 0.0656 | 5.4308 | -9.536 | 8896 |
| $n_E = 3$ | | | |
| 0 | 5.3849 | -101.2 | $3.655\times10^7$ |
| 0.0656 | 5.4308 | -9.280 | 8874 |
| Aiga P1[2] | | | |
| 0 | 5.7540 | -8.4579 | |
| 0.0656 | | -9.1219 | |
| Aiga P2[2] | | | |
| 0 | 5.5741 | -8.4342 | |
| 0.0656 | | -9.0968 | |
| Rozyczko and Bartlett[59] Min | | | |
| 0 | | -9.84 | 306 |
| 0.0656 | | **-8.04 ± 0.5** | **462 ± 40** |
| Rozyczko and Bartlett[59] Max | | | |
| 0 | | -12.87 | 378 |
| 0.0656 | | **-9.04 ± 0.5** | **711 ± 40** |
| Dudley and Ward[15;59] | | | |
| 0.0656 | | **11± 1** | **840± 120** |

the hyperpolarizabilities of HF. Regardless of our agreement with experiment, our agreement with theory means we can perform prelminary calculations of the first hyperpolarizability for molecules. Given that the second hyperpolarizabilities we calculated are an order of magnitude large than the values found in the literature, it is not beneficial to do a direct comparison. However, we will recall that when extended out to 40 or more states the cc-pVTZ basis began to oscillate around a value that could match Rozyczko and Bartlett's calculation in the cc-pVTZ basis. This agreement with Rozyczko and Bartlett, however, means we will likely disagree with experimental results as well. To properly get a result worth comparing in the third-order, we need to continue to explore the influences of the number of states on the hyperpolarizabilities.

With a fair assessment of our calculations compared against the literature, we move to

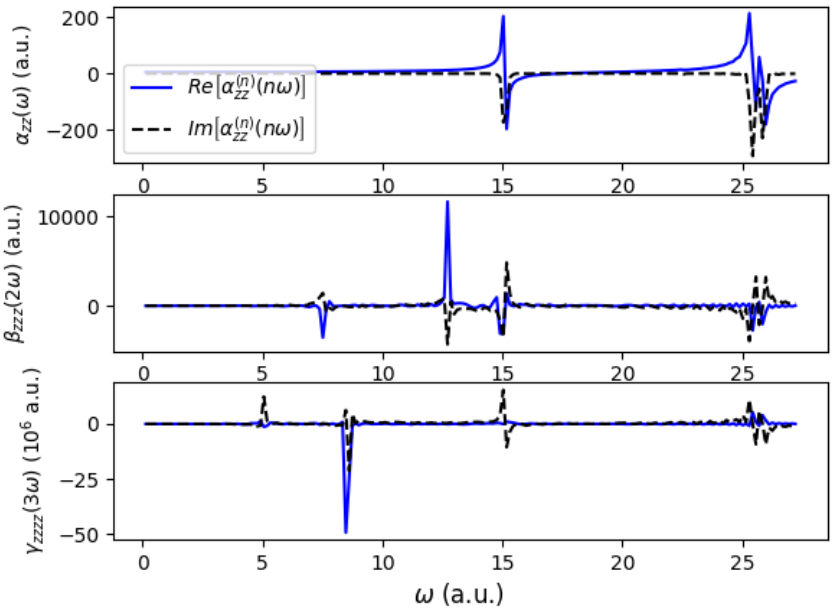


**Figure 3.8**: *Frequency responses of the (hyper)polarizabilities of HF up to $\omega = 1.0$ a.u. Across the three plots, we see peaks emerge at frequencies corresponding to excited state energies as well as at approximately half those energies for the first hyperpolarizability, and at one third those energies for the second hyperpolarizability.*

consider what is likely a more qualitative result. While still using a single regression point, we will evaluate the (hyper)polarizabilities across all frequencies in the domain $\omega = (0, 1.0]$ a.u. These calculations are presented in Fig 3.8. The frequency response of the polarizability is as we might expect given the perturbative formula: large peaks at frequencies approaching the excited state energies with large imaginary components at those frequencies. These peaks then begin to bunch up as we approach $\omega = 1.0$ a.u. which matches the behavior of the excited states.

The first and second hyperpolarizabilities exhibit similar behavior, but now there are more peaks. This matches what we would predict when using the perturbative formula as a reference. In the case of the first hyperpolarizability, there is an initial set of peaks that emerge at half of the excited state energies and then we see them where the excited state energies are located as we did in the polarizability. The second polarizability exhibits

something strange. According to the perturbative formula, we expect peaks to occur around $\Omega_n$, $\Omega_n/2$, and $\Omega_n/3$, where $\Omega_n$ is the energy of the $n$th excited state. Examining the frequency spectrum for the second hyperpolarizability, however, shows these peaks occuring at $\Omega_n$ and $\Omega_n/3$ only. While these peaks could be remarkably small, the more likely cause is numerical error from the sensitivity in third order calculations.

# Chapter 4

# Methyl oxirane

## 4.1 Chirality

When the reflection of a molecule cannot be superimposed upon the original molecule, we refer to that molecule as chiral. For each version of the molecule, we designate a "handedness" which is defined via its interaction with circularly polarized light. As such, each molecule is labeled as either "R-" or "S-". While interesting on its own, the importance of chirality becomes more apparent in biological systems. Many amino acids, sugars, aromatics, and various other biological molecules[28], including pharmaceuticals[13], are chiral. In fact, two enantiomers of the molecule may interact differently in the human body[13]. The most prevalent example of this is thalidomide[68].

Thalidomide was a drug developed to treat morning sickness in women; however, the children of the women took the drug were born with birth defects[11]. Further investigation led to the revelation that while one enantiomer treated morning sickness, the other led to the birth defects[68]. This tragedy highlights many motivations to study chirality and develop the ability to efficiently distinguish and sort different enantiomers of the same molecule.

### 4.1.1 Hyperpolarizability in Chiral Molecules

Chiral molecules are inherently non-centrosymmetric, so when studying the nonlinear effects of these molecules, they will produce a second-order response[49]. Furthermore, when in an isotropic solution, chiral molecules will still exhibit this second-order response provided it is not racemic[14]. This is inherent asymmetry in the molecules which makes second harmonic microscopy available for studying biological systems.

Much work has already gone into studying the nonlinear effects in chiral molecules. Champagne et al. have investigated three-wave mixing (TWM) in propylene oxide, another name for methyl oxirane[14]. Although we are studying the same molecule, we put emphasis on SHG and THG rather than the generic TWM. Additionally, they look at the permutations of $\beta_{xyz}$[14]. While it is important to note their work, we will be unable to directly compare our calculations.

By understanding the optical behavior of chiral molecules in the nonlinear regime, we may identify new ways to study them. Even better, we may find new ways to identify them and identify the ratio of enantiomers in a solution. Given that a racemic solution of chiral molecules will not exhibit second-order nonlinear effects, the strength of a nonlinear effect may be related to the ratio of the enantiomers in solution.

## 4.2 Hyperpolarizability of Methyl oxirane

### 4.2.1 Computational Details

We now turn to the chiral molecule of interest, methyl oxirane, which has the chemical formula $C_3H_6O$. Before calculating any of the molecular properties we need for hyperpolarizabilities, we must consider the enantiomer and orientation of the molecule. For our purposes, we have chosen to work with the right-handed enantiomer with the oxygen in the negative y-direction. Figure 4.1 depicts the exact orientation of the molecule in cartesian

space. With the enantiomer and orientation decided, we calculated the exicited state energies and dipole matrix elements using the EOM-CCSD program[33] from Molpro[70–72]. We then calculated the hyperpolarizabilities in the same manner as HF.

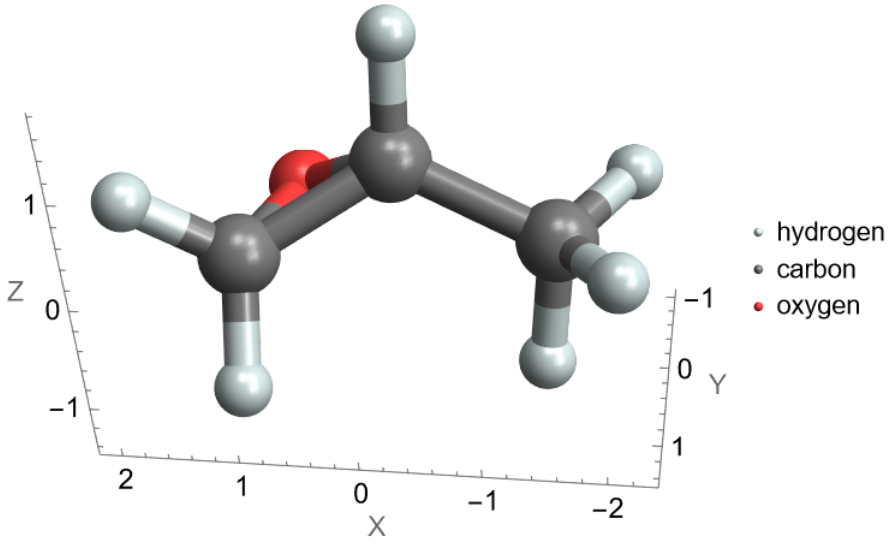


**Figure 4.1**: *The orientation of (R)-methyl oxirane in cartesian space used when calculating the excited state energies and dipole matrix elements.*

First, we considered how the (hyper)polarizabilities would converge with respect to the number of states for several basis sets. In particular, we looked at the Dunning's cc-pVTZ, aug-cc-pVTZ, cc-pVQZ basis sets as well as the ano-pVTZ basis set[43] which was collected from Basis Set Exchange[16;55;62], and Pople's 6-311++G** basis. For these initial calculations, we use a field with a strength of $|E_0| = 10^{-3}$ a.u. polarized along z axis with $\omega = 0.0656$ a.u. A single regression point is used in the calculations as well. For simplicity, we concentrate on the results of the $\alpha_{zz}$, $\beta_{zzz}$, and $\gamma_{zzzz}$ components. In these calculations, we limit ourselves to a maximum of 16 states due to a combination of factors. First, as we saw in HF, stable regions could be identified with at least one basis within 16 states. Second, the more complex molecule requires significantly longer computation time both in terms of calculating the dipole matrix elements and energies as well as the NLA procedures.

At first glance, the results for the polarizability from figure 4.2 states is rather chaotic. For each basis set, the values of the polarizabilities continue to climb even at the 16-state system

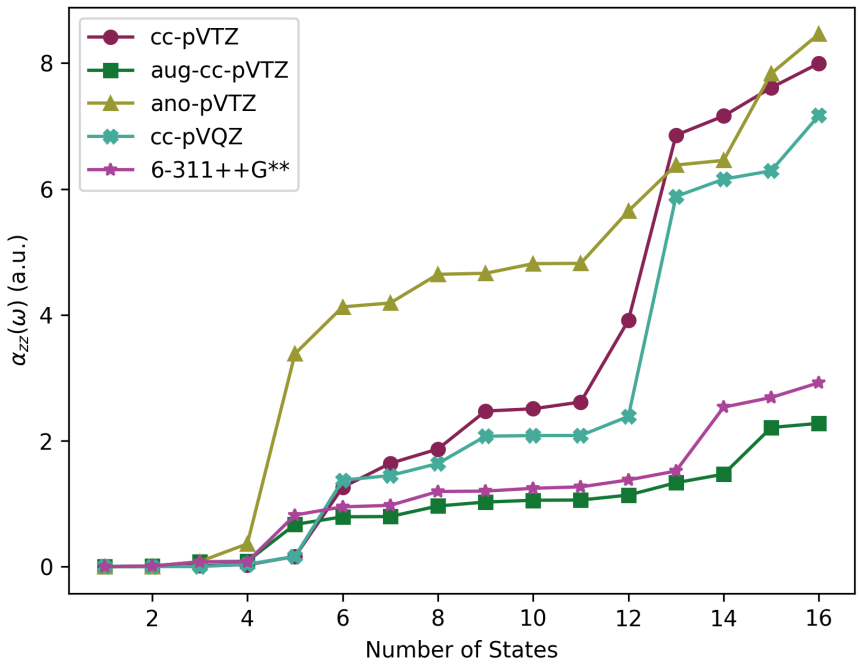


**Figure 4.2**: *Plot of the polarizability of methyl oxirane up to the first 16 states with several basis sets. For most basis sets, we see a sharp increase by the time we reach our final state. The cc-pVTZ basis shows a continual increase, however the jumps in value have reduce to be approximately 0.3 a.u. between states 15 and 16. On the other end, the aug-cc-pVTZ basis increases much more slowly keeping the first decimal constant between states 15 and 16. All other basis sets fall between these two extrema.*

point. While we clearly must extend the number of states we use for a proper calculation, we can still extract useful information from these results. The polarizability values calculated with the aug-cc-pVTZ basis increase the most gradually out of all basis sets. From 5 to 14 states, the polarizability calculated with this basis grows by at most 0.2 a.u. between states. Between 15 and 16 states, the polarizability varies by only 0.06 a.u. Similarly, the 6-311++G** basis grows considerably more gradually than the cc-pVTZ, ano-pVTZ, and cc-pVQZ bases, however, it does not reach the same level of consistency between the 15 and 16 state systems. Instead, we see these values of the polarizability differ by 0.3 a.u. Despite the rapid growth, we see this same difference between the 15- and 16-state systems in the cc-pVTZ basis. It is feasible, then, that many of these bases are approaching convergence,

and only require a handful more states.

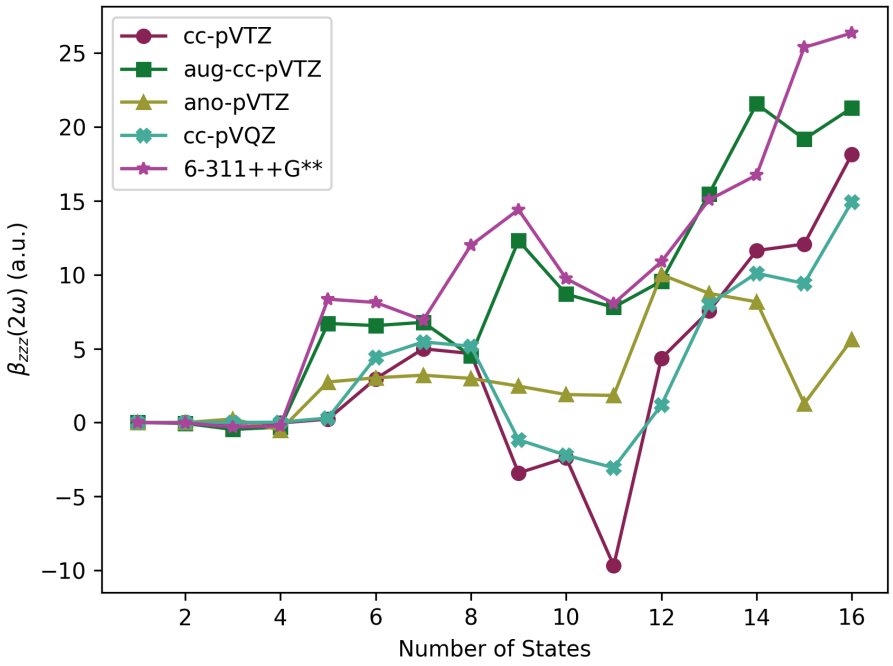


**Figure 4.3**: *Plot of the first hyperpolarizability of methyl oxirane up to the first 16 states with several basis sets. By 16 states, the results for all of these basis sets extend towards sharp increases. The least severe of these increases comes from the 6-311++G** basis, where there is only a 3.77% difference between the final two values. Additionally, the aug-cc-pVTZ basis oscillates between approximately 21 a.u. and 19 a.u. indicating that more states would lead to a converged value.*

The results for the first hyperpolarizability, featured in figure 4.3 are more chaotic than those for the polarizability. The first basis to address is the aug-cc-pVTZ basis. The first hyperpolarizability rapidly grows up until 14 states, at which point the results from this basis begin to oscillalte between 21.5 a.u. and 19.2 a.u. with the results for the 14- and 16-state systems differing by less than one percent. The ano-pVTZ basis appears that it may also be beginning to oscillate around the same number of states. In the case for this basis, the first hyperpolarizability varies between 8.16 a.u. and 1.28 a.u. We should also note that the 6-311++G** basis grows much more slowly between the 15- and 16-state systems than the cc-pVTZ and cc-pVQZ bases. The first hyperpolarizability grows by 3 a.u. in the Pople basis

while the Dunning basis result in the first hyperpolarizability growing by 5 a.u. to 6 a.u. Overall, we are faced with the fact that while some of these bases may approach convergence, we need to expand our calculations to include several more states for full assurance.

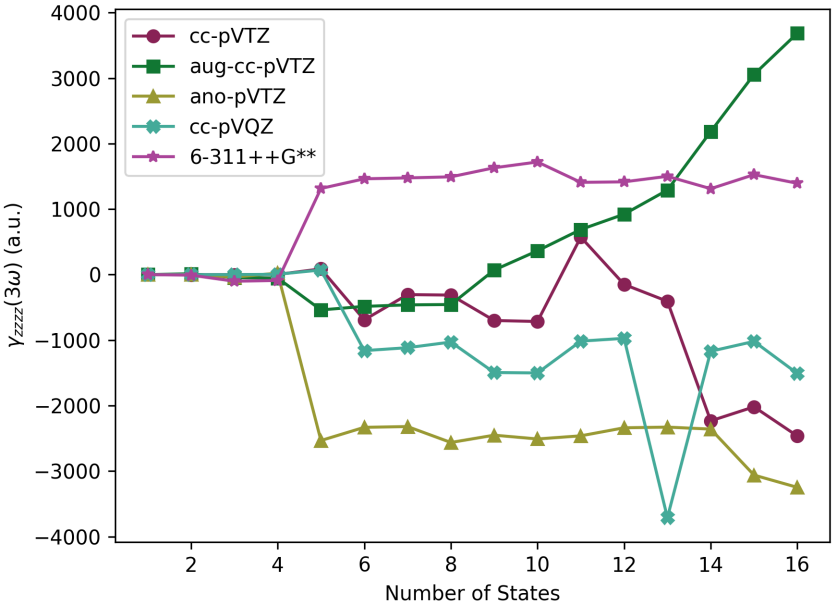


**Figure 4.4**: *Plot of the second hyperpolarizability of methyl oxirane up to the first 16 states with several basis sets. Unlike the polarizability and first polarizability, the results here are much better behaved, though it is not clear if that is due to numerical error. The most notable basis set, however is the 6-311++G** basis. By the inclusion of 5 states, this basis stablizes and oscillates between approximately 1300 a.u. and 1700 a.u. The value at 16 stats is 1394 a.u., which has a 5.83% difference from the 5 state result. The ano-pVTZ basis provides another interesting set of results. Between 5 and 14 states, the results vary from -2319 a.u. and -2509 a.u. but then they dip down to -3248 a.u. Finally, barring an excessive dip at 13 states, the cc-pVQZ basis osscillates between -1029 a.u. and -1508 a.u.*

The state convergence for the second hyperpolarizability, seen in figure 4.4 is remarkably more orderly when compared to the lower-order coefficients. It is unclear why this may be. It is possible that it is a side effect of the numerical sensitivities that occur when calculating the third-order coefficients. Alternatively, there may be something about methyl oxirane that leads to this result, but that is far less likely. Regardless, when investigating our most stable result, which comes from the 6-311++G** basis is converged to 94.4% of the final

value, though given the magnitude of these results, this still means they vary up to their tens place. Over this range of states, the second hyperpolarizability reaches a maximum of 1631 a.u. and a minimum of 1312 a.u. The ano-pVTZ basis also remains remarkably stable up until state 15, where it suddenly dips further negative. Before this dip, the second hyperpolarizability stays in the range of -2500 a.u. to -2300 a.u. Finally, the cc-pVQZ basis presents another curious case. Ignoring the massive dip around the 13-state system, the second hyperpolarizability is relatively stable, oscillating in the range of -1500 a.u. to -900 a.u. While that is a sizeable gap, the third-order coefficient only exits that range once after reaching the 6-state mark. We are again seeing trends that prompt further investigation into the influence of the states on the hyperpolarizability.

In our review of the convergence plots, we have found many reasons to continue considering the influence of the states on the (hyper)polarizabilities. However, computational limitations prevent this. Recall that the NLA requires us to solve the Liouville equation, which is a matrix differential equation. For any system, we solve for $n^2$ componentst that make up our density matrix. At 16 states, we are solving for 256 matrix components. While not performing a proper regression, these calculation will significantly more time, as we increase the number of points we use in our polynomial fits, this time will significantly increase. This is in conjunction with the time to calculate the molecular properties, which for many more states will take multiple days.

Instead of being halted by computational limitations, we shall investigate the (hyper)polarizabilities of methyl oxirane modeled as a 4-, 8-, 12-, and 16-state system. For this investigation, we shall use the 6-311++G** basis. We choose to use this basis both because of the surprising stability it exhibits for third-order calculations and because this is the basis used by Champagne[14]. While Champagne's results may not be directly applicable, they may still work as a good order of magnitude check for the first hyperpolarizability.

Next, we consider the response of the optical coefficients to various electric field strengths. For these calculations, we continue with the same frequency and basis set as previously

mentioned. Looking at figure 4.5, we see that it is primarily the second and third-order coefficients that have volatile reactions to a changing electric field. However, by carefully examining the plots, we see that at higher field strengths, the optical coefficients begin to increase as well. Using the plots to guide our decisions, the same field strength as used for HF, $|E_0| = 4 \times 10^{-4}$ a.u. seems to still be an appropriate value. Additionally, this makes us consistent with our previous calculations as well as the Nakano calculations.

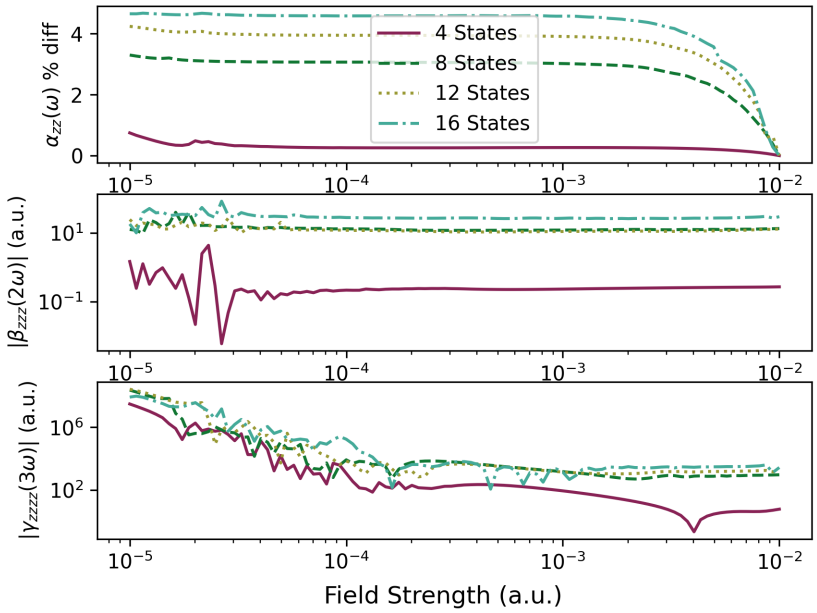


**Figure 4.5**: *Plots of the polarizability (top), first hyperpolarizability (middle), and second hyperpolarizability (bottom) to electric field strengths for , 8-, 12-, and 16-state methyl oxirane.*

Finally, we consider the effect of the number of regression points on the optical coefficients. The results of these tests can be found in figure 4.6. The polarizability is not strongly influenced by the number of regression points. At most, in the case of the 8-, 12-, 16-state systems, the polarizability is only changed at the fourth decimal place. The first hyperpolarizability for those same systems varies more, being altered in the first decimal place. Expectedly, the second hyperpolarizability is greatly affected by the influence of regression points, changing their value on the order of $10^3$. In this case, there is no one

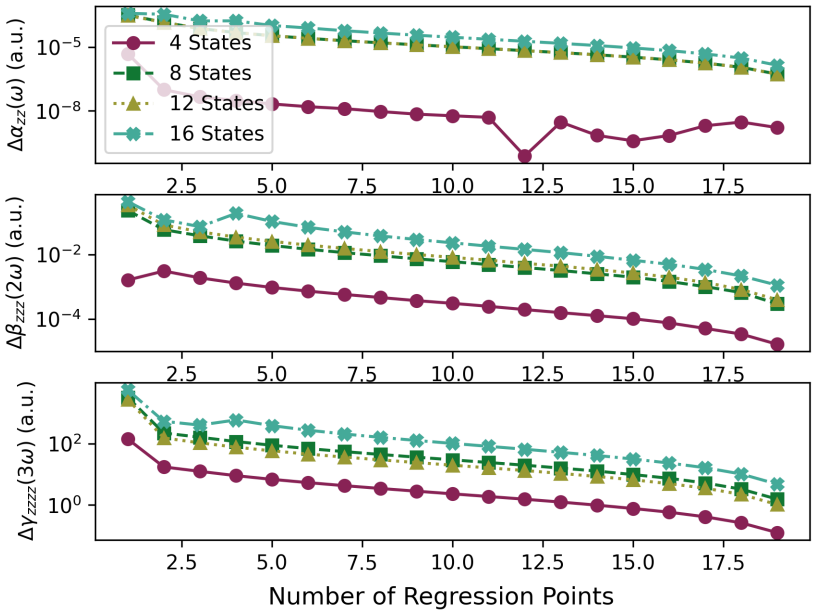


**Figure 4.6**: *Plots depicting the difference between the (hyper)polarizabilities calculated with an arbitrary $n_E$ points and the (hyper)polarizability calculated with 20 points. The top plot depicts the polarizability, the middle depicts the first hyperpolarizability, and the bottom depicts the third hyperpolarizability.*

correct answer for how many states to use. In an attempt to balance computation time and accuracy, we will opt to use $n_E = 6$.

As an example of our fits, Fig 4.7 depicts the fits for 16-state methyl oxirane at $n_E = 6$. Again, we have not calculated a $\chi^2$ value to measure the quality of our fits. However, an examintation by eye shows that the fits are in good agreement with the six points that were used.

### 4.2.2 Results and Discussion

To begin our discussion, we will consider our results for the polarizability calculated at $\lambda = 1094$ nm, which can be found in table 4.2.2. Examining the results, there are two striking details to consider. First, the polarizability tensor takes the form of a symmetric matrix, which is to be expected. Recall that the polarizability is directly proportional to

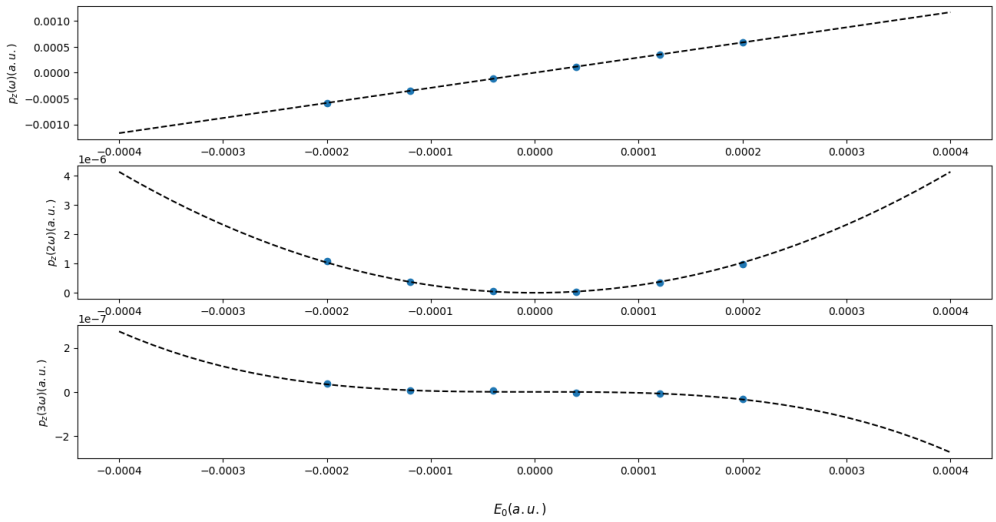


**Figure 4.7**: *Plots of six* $(E_0, p_i(n\omega))$ *points for methyl oxirane ranging from* $-E_0$ *to* $E_0$ *used for fitting the* $n$*th order polynomials for each order. The coefficients calculated for these fits show fair agreement with the points used for the fits.*

**Table 4.1**: *Components of the polarizability tensor calculated for the 4-, 8-, 12-, and 16-state system at a frequency corresponding to* $\lambda = 1064$ *nm.*

| $\alpha_{ij}(\omega)$ | 4-state | 8-state | 12-state | 16-state |
|---|---|---|---|---|
| $\alpha_{xx}(\omega)$ | 0.4688 | 1.229 | 3.037 | 3.280 |
| $\alpha_{xy}(\omega)$ | 0.6005 | 0.7419 | 0.4969 | 0.5006 |
| $\alpha_{xz}(\omega)$ | -0.0939 | 0.6193 | 0.3029 | 0.7623 |
| $\alpha_{yx}(\omega)$ | 0.6004 | 0.7416 | 0.4964 | 0.5006 |
| $\alpha_{yy}(\omega)$ | 1.391 | 1.902 | 2.305 | 2.368 |
| $\alpha_{yz}(\omega)$ | 0.0374 | 0.2156 | 0.2931 | 0.1126 |
| $\alpha_{zx}(\omega)$ | -0.0940 | 0.6192 | 0.3029 | 0.7618 |
| $\alpha_{zy}(\omega)$ | 0.0373 | 0.2154 | 0.2920 | 0.1110 |
| $\alpha_{zz}(\omega)$ | 0.0751 | 1.160 | 1.339 | 2.954 |

the electric susceptibility which is a symmetric tensor. The second thing to take note of is the rate of convergence for certain components. In particular consider $\alpha_{xx}$, $\alpha_{xy}$, and $\alpha_{yy}$. Between the 12- and 16-state results, these components and their transpose seem to be pointing towards convergence. For each of these components, the percent differences between the 12- and 16-state results are 7.69%, 0.74%, and 2.71% respectively with $\alpha_{yy}$ seemingly converged to the first decimal place.

Our results once again remind us that further exploration into the number of states is

**Table 4.2**: *Select components of the first hyperpolarizability tensor calculated for the 4-, 8-, 12-, and 16-state system at a frequency corresponding to* $\lambda = 1064$ *nm.*

| $\beta_{ijj}(2\omega)$ | 4-state | 8-state | 12-state | 16-state |
|---|---|---|---|---|
| $\beta_{xxx}(2\omega)$ | -0.427 | 1.92 | -4.80 | -2.15 |
| $\beta_{xyy}(2\omega)$ | -14.6 | -18.5 | -19.6 | -18.1 |
| $\beta_{xzz}(2\omega)$ | 0.014 | 1.52 | -14.4 | -13.3 |
| $\beta_{yxx}(2\omega)$ | -4.23 | -2.66 | 0.816 | 0.161 |
| $\beta_{yyy}(2\omega)$ | -21.4 | -20.045 | -27.8 | -26.8 |
| $\beta_{yzz}(2\omega)$ | -0.249 | -2.27 | 1.97 | -2.52 |
| $\beta_{zxx}(2\omega)$ | -0.264 | -1.70 | 3.58 | 7.08 |
| $\beta_{zyy}(2\omega)$ | 3.42 | -1.61 | 8.07 | 10.4 |
| $\beta_{zzz}(2\omega)$ | -0.207 | 10.6 | 9.41 | 22.8 |

required. Regardless, if we consider the 16-state system's results to be roughly accurate in comparison to a more thorough calculation, our results shed light on interesting properties for methyl oxirane. In an experiment, the individual components of the polarizability tensor will not be measured. Instead, they are more likely to measure an average polarizability $\overline{\alpha}$, which is defined as one $Tr[\alpha(\omega)]/3$. Applying this to our results we, we find the average polarizability is $\overline{\alpha} = 2.867$ a.u. We note that this serves primarily as a preliminary calculation, and not a final value. At the very least, we reasonably expect the same order of magnitude from experiments.

In table 4.2.2, we present our final results for the first hyperpolarizability. Again, there are a few interesting components to note from what we have calculated. First, the $\beta_{xyy}$ component only exhibits an 8.02% difference between the 12- and 16-state system and a 2.18% difference between the 8- and 16-state system. Similarly, we see this kind of behavior in the $\beta_{xzz}$ component as well as the $\beta_{yyy}$. It is not clear why these specific components would seem to begin converging more readily than the others beyond a numerical quirk. The results from Champagne for $\beta_{xyz}$ and the permutations of such were consistent across the sign and magnitude with all of their results being positive and on the order of 50. Our results, however, show less consistency, with orders of magnitude ranging from unity to 10 and there being a good mix of positive and negative values.

Experimentally, these results are less immediately useful. However, if we assume the

**Table 4.3**: *Tabulation and comparison of $\beta_{||}$ calculated across several wavelengths in this work as well as from the Champagne results.*

| $\lambda(nm)$ | 1970 | 1064 | 694.3 |
|---|---|---|---|
| This Work | -223 | -241 | -289 |
| Champagne[14] | -135 | -160 | -251 |
| % Diff | 49.2% | 40.4% | 14.1% |

16-state system is roughly accurate, we can calculate the the hyperpolarizability parallel to the electric dipole[14] $\beta_{||}$. Leveraging Kleinman's symmetry, we calculate $\beta_{||}$ as

$$\beta_{||} = \frac{3}{5}\sum_{3}^{ijk}\frac{\mu_i\beta_{ijj}}{|\mu_k|} \tag{4.1}$$

This is what is more often measured in experiments[64]. Calculating the parallel hyperpolarizability, we get that $\beta_{||} = -240.5$ a.u. This result is significantly larger than Champagne's result of $-160 a.u.$[14] As Champagne has calculated the parallel hyperpolarizability across several wavelengths, we shall do the same and compare the results. Table 4.2.2 summarizes these results. In general, our estimations of $\beta_{||}$ are larger than those calculated by Champagne. There are at least two sources we can attribute this difference two: optical effects and differing levels of theory. First, recall that Champagne is studying the more general case of TWM. Furthermore, they only include single excitations in their level of theory while we include single and double excitations.

Our calculations for the second hyperpolarizability are found in table 4.2.2, and they are more scattered across values between the various systems we investigated. Several of these components show a consistent sign across the 12- and 16-state systems, with some even managing consistency into the 8-state system. Unfortunately, the sign and order of magnitude may be the only pieces of information we are able to extract without the ability to compare against anything. Experimentally, the components we calculated would likely not be measured. Rather, experimentalists would see measurements of the parallel and perpendicular parts of the second hyperpolarizability or the isotropic average due to the

**Table 4.4**: *Select components of the second hyperpolarizability tensor calculated for the 4-, 8-, 12-, and 16-state system at a frequency corresponding to* $\lambda = 1064$ *nm.*

| $\gamma_{ijjj}(3\omega)$ | 4-state | 8-state | 12-state | 16-state |
|---|---|---|---|---|
| $\gamma_{xxxx}(3\omega)$ | -64.9 | -1087 | -4220 | -3363 |
| $\gamma_{xyyy}(3\omega)$ | -408 | -385 | -338 | -756 |
| $\gamma_{xzzz}(3\omega)$ | 173 | -532 | -1131 | -1350 |
| $\gamma_{yxxx}(3\omega)$ | 190 | 16.7 | -952 | -584 |
| $\gamma_{yyyy}(3\omega)$ | -1850 | -2301 | -3578 | -2039 |
| $\gamma_{yzzz}(3\omega)$ | -97.4 | 109 | -955 | -168 |
| $\gamma_{zxxx}(3\omega)$ | 57.7 | -19.2 | -393 | -788 |
| $\gamma_{zyyy}(3\omega)$ | -10.1 | 446 | 146 | 272 |
| $\gamma_{zzzz}(3\omega)$ | -42.6 | 159 | -631 | -1477 |

isotropy of gasses and liquids[64]. With the components we have calculated, we are unable to actually calculate these as well. However, by averaging the components we do have, we can provide a rough estimate of the isotropic average. Doing this, we estimate the isotropic average to be -1319 a.u. Now, this estimate comes with caviats. Primarily, we are limited by the number of states we have used and the numerical sensitivities in the third-order coefficient, which has been a theme through this thesis. Keeping this in mind, our result does not seem entirely unreasonable. Many molecules have their second hyperpolarizability in that order of magnitude (see Shelton[64] and Bishop[7] for tables). Thus, experimentally, researchers would be looking for a usual signal in the third order response.

The results we have presented are the molecular frame (hyper)polarizabilities of methyl oxirane. Although Shivaram has presented a method for directly probing these components, their method is flawed when the molecule does not have a identifiable set of symmetry axes. Their method relies on being able to relate the lab frame susceptibility to the hyperpolarizabilities and angle of the molecule's symmetry axis with the polarization of the incident fields. While for a molecule with defined symmetry axes, this expression may be reduced to include only a handful of the tensor elements, an asymmetric molecule will require all tensor elements. Additionally, with no clear symmetry axis, the sensible choice is to use the permanent dipole as the "molecular axis" for measuring the angle with respect to incident fields. This choice, however, leaves the molecule's rotation about that dipole axis

ambiguous. In reality, for a molecule like methyl oxirane, experiment would measure the hyperpolarizabilities rotationally averaged about the dipole axis.

Instead of measuring the molecular frame component themselves, experiment should focus on measuring the susceptibility of isotropic distributions of methyl oxirane in the gas or liquid phase. In particular, experiments should focus on studying the SHG response in methyl oxirane since that should be the first apparent nonlinear signal. For these experiments, we have provided an estimate of what their experiment should find when measuring $\beta_{||}$ for various wavelengths in Table 4.2.2.

# Chapter 5

# Conclusion

Throughout this thesis, we have studied the (hyper)polarizabilities of two molecules: hydrogen fluoride and methyl oxirane. While our studies on hydrogen fluoride were primarily meant as a gauge of our computational abilities, we uncovered crucial details. Our calculations in the first and second order coefficients matched to similar results from the literature. The polarizability matched with a maximum of a 5.38% difference and a minimum of 3.37% when compared to the Hartree-Fock limit. The first hyperpolarizability was more greatly influenced by numerical noise, resulting in a maximum percent difference of 17.06% and minimum of 2.62%. The second hyperpolarizability was even more strongly influenced by numerical noise and the inclusion of states, finding that upwards of 40 states are needed for proper computations of the second hyperpolarizability. Clearly, more effort needs to be focused on calculations of the second hyperpolarizability. Despite this, we showed our capabilities for calculating the polarizability and first hyperpolarizability for molecules, and continued to work with methyl oxirane.

The need for many more states than previous reviews on the NLA became more apparent in our investigation of methyl oxirane. In our intial calculations, we saw at most weak convergence in the initial 16 states, with many of the trends encouraging further exploration into the number of states. Despite, this we continued calculations for 4-, 8-, 12-, and 16-state

models of methyl oxirane. Ultimately the results of the 16-state model presented a range of values which seemed reasonable to find in an experiment. Specifically, we found that the average polarizability was on the order of unity. Our calculations for the parallel component of the first hyperpolarizability were larger than those found in the literature across multiple wavelengths. Our results preliminary results for the second hyperpolarizability hinted that methyl oxirane exhibites a fairly common value on the order of -1000 $a.u.$

Because chiral molecules are known for their second order response in isotropic solutions, experiments should focus on measuring first hyperpolarizability of methyl oxirane. Using a static electric field, the molecular dipoles may be aligned with the polarization of the field. Subsiquent laser pulses can then be used to generate second harmonics and measure the parallel component of the first hyperpolarizability. From our calculations, we predict $\beta_{||}(SHG)$ to be on the order of -200 a.u. For an exact comparison, further calculations are required.

There are several avenues for the continuation of this project. Beyond expanding the code to calculate all tensor componnets of the hyperpolarizabilities, our work showed the need for further investigation of the number of states used in the NLA. We saw the need for several more states than the literature suggested, with methyl oxirane showing no clear convergence within 16 states. To further bolster this analysis, a comparative study of the number of states needed for the NLA and the SOS method would shed light on the exact influence of states.

Beyond the number of states we work with, the choice of basis in our calculations for molecular properties should be investigated further. In this work, we have shown that the exact choice in basis can greatly affect the value of the hyperpolarizability we calculate. While more basis sets and larger basis sets should be studied, the development of a basis set for the hyperpolarizability of methyl oxirane should also be considered.

# Bibliography

[1] Abraham, T., Kayra, D., McManus, B., and Scott, A. (2012). Quantitative assessment of forward and backward second harmonic three dimensional images of collagen type i matrix remodeling in a stimulated cellular environment. *Journal of Structural Biology*, 180(1):17–25.

[2] Aiga, F., Sasagane, K., and Itoh, R. (1992). The quadratic response function in the thfd approximation and its application to frequency-dependent hyperpolarizabilities of the fh molecule. *Chemical Physics*, 167(3):277–290.

[3] Akkiraju, H., price, C., Wang, L., Caplan, J., and Nohe, A. (2015). Analysis of trabecular bone architecture using two photon fluorescence microscopy. *Biophysical Journal*, 108(2, Supplement 1):325a.

[4] Anwar, A., Perumangatt, C., Steinlechner, F., Jennewein, T., and Ling, A. (2021). Entangled photon-pair sources based on three-wave mixing in bulk crystals. *Review of Scientific Instruments*, 92(4):041101.

[5] Bishop, D. M. (1990). Molecular vibrational and rotational motion in static and dynamic electric fields. *Rev. Mod. Phys.*, 62:343–374.

[6] Bishop, D. M. and Kirtman, B. (1991). A perturbation method for calculating vibrational dynamic dipole polarizabilities and hyperpolarizabilities. *The Journal of Chemical Physics*, 95(4):2646–2658.

[7] Bishop, D. M. and Norman, P. (2001). Chapter 1 - calculations of dynamic hyperpolarizabilities for small and medium-sized molecules. In Singh Nalwa, H., editor, *Handbook*

*of Advanced Electronic and Photonic Materials and Devices*, pages 1–62. Academic Press, Burlington.

[8] Boyd, R. W. (2020a). Chapter 1 - the nonlinear optical susceptibility. In Boyd, R. W., editor, *Nonlinear Optics (Fourth Edition)*, pages 1–64. Academic Press, fourth edition edition.

[9] Boyd, R. W. (2020b). Chapter 3 - quantum-mechanical theory of the nonlinear optical susceptibility. In Boyd, R. W., editor, *Nonlinear Optics (Fourth Edition)*, pages 137–202. Academic Press, fourth edition edition.

[10] Bruno, N., Martin, A., and Thew, R. (2014). Generation of tunable wavelength coherent states and heralded single photons for quantum optics applications. *Optics Communications*, 327:17–21. Special Issue on Nonlinear Quantum Photonics.

[11] Burley, D. and Lenz, W. (1962). Thalidomide and congenital abnormalities. *The Lancet*, 279(7223):271–272. Originally published as Volume 1, Issue 7223.

[12] Campagnola, P. J., Millard, A. C., Terasaki, M., Hoppe, P. E., Malone, C. J., and Mohler, W. A. (2002). Three-dimensional high-resolution second-harmonic generation imaging of endogenous structural proteins in biological tissues. *Biophysical Journal*, 82(1):493–508.

[13] Ceramella, J., Iacopetta, D., Franchini, A., De Luca, M., Saturnino, C., Andreu, I., Sinicropi, M. S., and Catalano, A. (2022). A look at the importance of chirality in drug activity: Some significative examples. *Applied Sciences*, 12(21).

[14] Champagne, B., Fischer, P., and Buckingham, A. (2000). Ab initio investigation of the sum-frequency hyperpolarizability of small chiral molecules. *Chemical Physics Letters*, 331(1):83–88.

[15] Dudley, J. W., I. and Ward, J. F. (1985). Measurements of second- and third-order nonlinear polarizabilities for hf and hcl. *The Journal of Chemical Physics*, 82(10):4673–4677.

[16] Feller, D. (1996). The role of databases in support of computational chemistry calculations. *J. Comput. Chem.*, 17:1571–1586.

[17] Franken, P. A., Hill, A. E., Peters, C. W., and Weinreich, G. (1961). Generation of optical harmonics. *Phys. Rev. Lett.*, 7:118–119.

[18] Freund, I., Deutsch, M., and Sprecher, A. (1986). Connective tissue polarity. optical second-harmonic microscopy, crossed-beam summation, and small-angle scattering in rat-tail tendon. *Biophysical Journal*, 50(4):693–712.

[19] Gergonne, J. (1974). The application of the method of least squares to the interpolation of sequences. *Historia Mathematica*, 1(4):439–447.

[20] Giustina, M., Versteegh, M. A. M., Wengerowsky, S., Handsteiner, J., Hochrainer, A., Phelan, K., Steinlechner, F., Kofler, J., Larsson, J.-A., Abellán, C., Amaya, W., Pruneri, V., Mitchell, M. W., Beyer, J., Gerrits, T., Lita, A. E., Shalm, L. K., Nam, S. W., Scheidl, T., Ursin, R., Wittmann, B., and Zeilinger, A. (2015). Significant-loophole-free test of bell's theorem with entangled photons. *Phys. Rev. Lett.*, 115:250401.

[21] Göppert-Mayer, M. (1931). Über Elementarakte mit zwei Quantensprüngen. *Annalen der Physik*, 401(3):273–294.

[22] Goulielmakis, E., Schultze, M., Hofstetter, M., Yakovlev, V. S., Gagnon, J., Uiberacker, M., Aquila, A. L., Gullikson, E. M., Attwood, D. T., Kienberger, R., Krausz, F., and Kleineberg, U. (2008). Single-cycle nonlinear optics. *Science*, 320(5883):1614–1617.

[23] Guo, Y., Ho, P. P., Savage, H., Harris, D., Sacks, P., Schantz, S., Liu, F., Zhadin, N., and

Alfano, R. R. (1997). Second-harmonic tomography of tissues. *Opt. Lett.*, 22(17):1323–1325.

[24] Hajiesmaeilbaigi, F., Razzaghi, H., Mahdizadeh, M., Moghaddam, M., and Ruzbehani, M. (2011). Design and construction of a 110w green laser for medical application. *Optics & Laser Technology*, 43(8):1428–1430.

[25] Hammond, B. L. and Rice, J. E. (1992). Ab initio determination of the nonlinear optical properties of hcl. *The Journal of Chemical Physics*, 97(2):1138–1143.

[26] Harris, S. E., Oshman, M. K., and Byer, R. L. (1967). Observation of tunable optical parametric fluorescence. *Phys. Rev. Lett.*, 18:732–734.

[27] Hong, C. K., Ou, Z. Y., and Mandel, L. (1987). Measurement of subpicosecond time intervals between two photons by interference. *Phys. Rev. Lett.*, 59:2044–2046.

[28] Inaki, M., Liu, J., and Matsuno, K. (2016). Cell chirality: its origin and roles in left-right asymmetric development. *Philosophical transactions of the Royal Society of London. Series B, Biological sciences*, 371(1710).

[29] Jackson, J. D. (1999). *Classical electrodynamics*. Wiley, New York, NY, 3rd ed. edition.

[30] Kerr, J. (1875a). Liv. a new relation between electricity and light: Dielectrified media birefringent (second paper). *The London, Edinburgh, and Dublin Philosophical Magazine and Journal of Science*, 50(333):446–458.

[31] Kerr, J. (1875b). Xl. a new relation between electricity and light: Dielectrified media birefringent. *The London, Edinburgh, and Dublin Philosophical Magazine and Journal of Science*, 50(332):337–348.

[32] Kobayashi, T., Sasagane, K., Aiga, F., and Yamaguchi, K. (1999). Calculation of frequency-dependent first hyperpolarizabilities using the second-order møller–plesset perturbation theory. *The Journal of Chemical Physics*, 110(24):11720–11733.

[33] Korona, T. and Werner, H.-J. (2003). Local treatment of electron excitations in the eom-ccsd method. *The Journal of Chemical Physics*, 118(7):3006–3019.

[34] Li, M., Wang, H., Li, X., Wang, J., Zhang, J., San, X., Ma, P., Lu, Y., Liu, Z., Wang, C., Yang, Y., Luo, S., and Ding, D. (2023). Stable attosecond beamline equipped with high resolution electron and xuv spectrometer based on high-harmonics generation. *Journal of Electron Spectroscopy and Related Phenomena*, 263:147287.

[35] Lin, Y.-C., Fidler, A. P., Sandhu, A., Lucchese, R. R., McCurdy, C. W., Leone, S. R., and Neumark, D. M. (2021). Coupled nuclear–electronic decay dynamics of o2 inner valence excited states revealed by attosecond xuv wave-mixing spectroscopy. *Faraday Discussions*, 228:537–554.

[36] Luo, Y., Ågren, H., Jørgensen, P., and Mikkelsen, K. V. (1995a). Response theory and calculations of molecular hyperpolarizabilities. In Löwdin, P.-O., editor, *Advances in Quantum Chemistry, Vol. 26*, volume 26 of *Advances in Quantum Chemistry*, pages 165–237. Academic Press.

[37] Luo, Y., Ågren, H., Minaev, B., and Jørgensen, P. (1995b). The hyperpolarizability of molecular oxygen. *Journal of Molecular Structure: THEOCHEM*, 336(1):61–67.

[38] Magde, D. and Mahr, H. (1967). Study in ammonium dihydrogen phosphate of spontaneous parametric interaction tunable from 4400 to 16 000 å. *Phys. Rev. Lett.*, 18:905–907.

[39] Mohammed, A. A. K., Limacher, P. A., and Champagne, B. (2013). Finding optimal finite field strengths allowing for a maximum of precision in the calculation of polarizabilities and hyperpolarizabilities. *Journal of Computational Chemistry*, 34(17):1497–1507.

[40] Nakano, M. and Yamaguchi, K. (1994). Numerical liouville approach: A calculation method for nonlinear optical susceptibilities of n-state systems. *Phys. Rev. A*, 50:2989–3004.

[41] Nakano, M., Yamaguchi, K., Matsuzaki, Y., Tanaka, K., and Yamabe, T. (1995a). Numerical liouville approach: Formulation of third-order nonlinear optical susceptibilities. *The Journal of Chemical Physics*, 102(7):2986–2995.

[42] Nakano, M., Yamaguchi, K., Matsuzaki, Y., Tanaka, K., and Yamabe, T. (1995b). Numerical liouville approach. third-order nonlinear optical susceptibilities in thg, efish and dfwm. *Chemical Physics Letters*, 233(4):411–419.

[43] Neese, F. and Valeev, E. F. (2011). Revisiting the atomic natural orbital approach for basis sets: Robust systematic basis sets for explicitly correlated and conventional correlated ab initio methods? *J. Chem. Theory Comput.*, 7:33–43.

[44] New, G. H. C. and Ward, J. F. (1967). Optical third-harmonic generation in gases. *Phys. Rev. Lett.*, 19:556–559.

[45] Nicolini, C., Celli, A., Gratton, E., and Winter, R. (2006). Pressure tuning of the morphology of heterogeneous lipid vesicles: A two-photon-excitation fluorescence microscopy study. *Biophysical Journal*, 91(8):2936–2942.

[46] Oheim, M., Michael, D. J., Geisbauer, M., Madsen, D., and Chow, R. H. (2006). Principles of two-photon excitation fluorescence microscopy and other nonlinear imaging approaches. *Advanced Drug Delivery Reviews*, 58(7):788–808. Multi-Photon Imaging: Diseases and Therapies.

[47] Olsen, J. and Jo/rgensen, P. (1985). Linear and nonlinear response functions for an exact state and for an mcscf state. *The Journal of Chemical Physics*, 82(7):3235–3264.

[48] Orr, B. and Ward, J. (1971). Perturbation theory of the non-linear optical polarization of an isolated system. *Molecular Physics*, 20(3):513–526.

[49] Ostroverkhov, V., Ostroverkhova, O., Petschek, R., Singer, K., Sukhomlinova, L.,

Twieg, R., Wang, S.-X., and Chien, L. (2000). Optimization of the molecular hyperpolarizability for second harmonic generation in chiral media. *Chemical Physics*, 257(2):263–274.

[50] Pandey, S., Tan, L. Z., Walz, F., Makhija, V., and Shivaram, N. (2024). Ultrafast temporal phase-resolved nonlinear optical spectroscopy in the molecular frame. *Optica*, 11(6):776–781.

[51] Pandey, S., Walz, F., and Shivaram, N. (2025). Femtosecond temporal phase-resolved nonlinear optical spectroscopy in molecules with lock-in enabled phase tracking.

[52] Paul, P. M., Toma, E. S., Breger, P., Mullot, G., Augé, F., Balcou, P., Muller, H. G., and Agostini, P. (2001). Observation of a train of attosecond pulses from high harmonic generation. *Science*, 292(5522):1689–1692.

[53] Pfeffer, C. P., Olsen, B. R., Ganikhanov, F., and François Légaré (2008). Multimodal nonlinear optical imaging of collagen arrays. *Journal of Structural Biology*, 164(1):140–145.

[54] Pluta, T. and Sadlej, A. J. (1998). Hypol basis sets for high-level-correlated calculations of electric dipole hyperpolarizabilities. *Chemical Physics Letters*, 297(5):391–401.

[55] Pritchard, B. P., Altarawy, D., Didier, B., Gibsom, T. D., and Windus, T. L. (2019). A new basis set exchange: An open, up-to-date resource for the molecular sciences community. *J. Chem. Inf. Model.*, 59:4814–4820.

[56] Puskar, N. G., Lin, Y.-C., Gaynor, J. D., Schuchter, M. C., Chattopadhyay, S., Marante, C., Fidler, A. P., Keenan, C. L., Argenti, L., Neumark, D. M., and Leone, S. R. (2023). Measuring autoionization decay lifetimes of optically forbidden inner valence excited states in neon atoms with attosecond noncollinear four-wave-mixing spectroscopy. *Phys. Rev. A*, 107:033117.

[57] Rice, J. E. and Handy, N. C. (1991). The calculation of frequency-dependent polarizabilities as pseudo-energy derivatives. *The Journal of Chemical Physics*, 94(7):4959–4971.

[58] Riesbeck, T. and Eichler, H. (2007). A high power laser system at 540nm with beam coupling by second harmonic generation. *Optics Communications*, 275(2):429–432.

[59] Rozyczko, P. and Bartlett, R. J. (1997). Frequency dependent equation-of-motion coupled cluster hyperpolarizabilities: Resolution of the discrepancy between theory and experiment for hf? *The Journal of Chemical Physics*, 107(24):10823–10826.

[60] Rupprecht, P., Puskar, N. G., Neumark, D. M., and Leone, S. R. (2024). Extracting doubly excited state lifetimes in helium directly in the time domain with attosecond noncollinear four-wave-mixing spectroscopy. *Phys. Rev. Res.*, 6:043100.

[61] Samanta, G., Chaitanya Kumar, S., Devi, K., and Ebrahim-Zadeh, M. (2012). High-power, continuous-wave ti:sapphire laser pumped by fiber-laser green source at 532nm. *Optics and Lasers in Engineering*, 50(2):215–219.

[62] Schuchardt, K. L., Didier, B. T., Elsethagen, T., Sun, L., Gurumoorthi, V., Chase, J., Li, J., and Windus, T. L. (2007). Basis set exchange: A community database for computational sciences. *J. Chem. Inf. Model.*, 47:1045–1052.

[63] Sekino, H. and Bartlett, R. J. (1986). Frequency dependent nonlinear optical properties of molecules. *The Journal of Chemical Physics*, 85(2):976–989.

[64] Shelton, D. P. and Rice, J. E. (1994). Measurements and calculations of the hyperpolarizabilities of atoms and small molecules in the gas phase. *Chemical Reviews*, 94(1):3–29.

[65] Shivaram, N., Thurston, R., Belkacem, A., Weber, T., Tan, L. Z., and Slaughter, D. S. (2026). Interplay between ultrafast electronic and librational dynamics in liquid nitrobenzene probed with two-color four-wave mixing. *The Journal of Physical Chemistry Letters*, 17(10):2911–2918.

[66] Shtoff, A. V., Dmitriev, Y. Y., and Rerat, M. (2005). Quasienergy derivative method

for the optical susceptibilities of molecules in the floquet theory. *Optics and Spectroscopy*, 99(4):545–551.

[67] Sun, H., Wang, S., Chen, J., and Yu, H. (2022). Label-free second harmonic generation imaging of cerebral vascular wall in local ischemia mouse model in vivo. *Neuroscience*, 502:10–24.

[68] Tokunaga, E., Yamamoto, T., Ito, E., and Shibata, N. (2018). Understanding the thalidomide chirality in biological processes by the self-disproportionation of enantiomers. *Scientific Reports*, 8(1):17131.

[69] Virtanen, P., Gommers, R., Oliphant, T. E., Haberland, M., Reddy, T., Cournapeau, D., Burovski, E., Peterson, P., Weckesser, W., Bright, J., van der Walt, S. J., Brett, M., Wilson, J., Millman, K. J., Mayorov, N., Nelson, A. R. J., Jones, E., Kern, R., Larson, E., Carey, C. J., Polat, İ., Feng, Y., Moore, E. W., VanderPlas, J., Laxalde, D., Perktold, J., Cimrman, R., Henriksen, I., Quintero, E. A., Harris, C. R., Archibald, A. M., Ribeiro, A. H., Pedregosa, F., van Mulbregt, P., and SciPy 1.0 Contributors (2020). SciPy 1.0: Fundamental Algorithms for Scientific Computing in Python. *Nature Methods*, 17:261–272.

[70] Werner, H.-J., Knowles, P. J., Celani, P., Györffy, W., Hesselmann, A., Kats, D., Knizia, G., Köhn, A., Korona, T., Kreplin, D., Lindh, R., Ma, Q., Manby, F. R., Mitrushenkov, A., Rauhut, G., Schütz, M., Shamasundar, K. R., Adler, T. B., Amos, R. D., Bennie, S. J., Bernhardsson, A., Berning, A., Black, J. A., Bygrave, P. J., Cimiraglia, R., Cooper, D. L., Coughtrie, D., Deegan, M. J. O., Dobbyn, A. J., Doll, K., Dornbach, M., Eckert, F., Erfort, S., Goll, E., Hampel, C., Hetzer, G., Hill, J. G., Hodges, M., Hrenar, T., Jansen, G., Köppl, C., Kollmar, C., Lee, S. J. R., Liu, Y., Lloyd, A. W., Mata, R. A., May, A. J., Mussard, B., McNicholas, S. J., Meyer, W., Miller III, T. F., Mura, M. E., Nicklass, A., O'Neill, D. P., Palmieri, P., Peng, D., Peterson, K. A., Pflüger, K., Pitzer, R., Polyak, I., Reiher, M., Richardson, J. O., Robinson, J. B., Schröder, B., Schwilk, M., Shiozaki, T.,

Sibaev, M., Stoll, H., Stone, A. J., Tarroni, R., Thorsteinsson, T., Toulouse, J., Wang, M., Welborn, M., and Ziegler, B. Molpro, version , a package of ab initio programs. see.

[71] Werner, H.-J., Knowles, P. J., Knizia, G., Manby, F. R., and Schütz, M. (2012). Molpro: a general-purpose quantum chemistry program package. *WIREs Computational Molecular Science*, 2(2):242–253.

[72] Werner, H.-J., Knowles, P. J., Manby, F. R., Black, J. A., Doll, K., Heßelmann, A., Kats, D., Köhn, A., Korona, T., Kreplin, D. A., Ma, Q., Miller, Thomas F., I., Mitrushchenkov, A., Peterson, K. A., Polyak, I., Rauhut, G., and Sibaev, M. (2020). The molpro quantum chemistry package. *The Journal of Chemical Physics*, 152(14):144107.

[73] Xia, C.-L., Liu, Q.-Y., and Miao, X.-Y. (2018). Theoretical investigation of the isolated attosecond pulse generation by restraining the spatial distribution of high-order harmonic emission. *Optics Communications*, 407:127–131.

[74] Yamamoto, S., Oshima, Y., Saitou, T., Watanabe, T., Miyake, T., Yoshida, O., Tokumoto, Y., Abe, M., Matsuura, B., Hiasa, Y., and Imamura, T. (2016). Quantitative imaging of fibrotic and morphological changes in liver of non-alcoholic steatohepatitis (nash) model mice by second harmonic generation (shg) and auto-fluorescence (af) imaging using two-photon excitation microscopy (tpem). *Biochemistry and Biophysics Reports*, 8:277–283.

[75] Zuev, M. B. and Nefediev, S. E. (2004). Rational design of atomic gaussian basis sets for ab initio calculations of the dipole polarizabilities and hyperpolarizabilities. i. optimized polarization sets for the first-row atoms from b to f. *Journal of Computational Methods in Sciences and Engineering*, 4(3):481–491.